A02-13803

AIAA 2002-0351
Effect of Applied Magnetic Field on the Instability of Mach 4.5 Boundary Layer over a Flat Plate

Felix Cheng and Xiaolin Zhong
University of California, Los Angeles, California

Sivaram Gogineni
Innovative Scientific Solutions, Inc., Dayton, Ohio

Roger L. Kimmel
Air Force Research Laboratory, Dayton, Ohio

40th Aerospace Sciences Meeting & Exhibit
14-17 January 2002 / Reno, NV

EFFECT OF APPLIED MAGNETIC FIELD ON THE INSTABILITY OF MACH 4.5 BOUNDARY LAYER OVER A FLAT PLATE

Felix Cheng * and **Xiaolin Zhong** †
University of California, Los Angeles, California
and
Sivaram Gogineni ‡
Innovative Scientific Solutions, Inc., Dayton, Ohio
and
Roger L. Kimmel §
Air Force Research Laboratory, Dayton, Ohio

1 Abstract

This paper investigates, by direct numerical simulation, the effects of an imposed magnetic field on a weakly ionized Mach 4.5 boundary layer. The main emphasis of the study is on MHD effects on the second mode instability in supersonic boundary layer. The imposed magnetic fields are generated by placing two-dimensional magnetic dipoles below of the flat plate surface. The gas is assumed to have a constant electrical conductivity of $100 mho/m$. The magnetic Reynolds number of the flow is small so that the induced magnetic field in the flow is neglected. The governing equations of the MHD flow, which are the Navier-Stokes equations with the applied magnetic force terms, are computed by a fifth-order shock-fitting numerical scheme. A series of cases with different imposed magnetic fields have been investigated on the influences of imposed magnetic field on both the mean flow and on the second mode stability. It is found that the imposed magnetic fields significantly retard the streamwise velocity and reduce the local skin friction in the mean flow. For the case of a strong imposed magnetic field, a local separation region is generated in the mean flow with a strong adverse pressure gradient. Meanwhile, the second mode wave disturbances are found to be stabilized by the imposed magnetic fields, even for the case with strong adverse pressure gradient and a local separated flow region. This unexpected strong stabilization of the second mode wave is believed to be caused by the alteration of the steady base flow by the magnetic field. It is also found that, unlike the second mode, the magnetic fields slightly destabilize the first mode waves because the different instability mechanisms of the two modes. The results presented in this paper are the first concrete results on the interaction of second instability mode with magnetic field in a supersonic boundary layer.

Nomenclature

$\mathbf{B}$	=	magnetic field vector
B_x, B_y, B_z	=	Cartesian magnetic field components
c	=	local speed of sound
C_v	=	constant volume specific heat
e	=	total energy of fluid
$\mathbf{E}$	=	electric field vector
J	=	Jacobian of grid transformation
$\mathbf{J}$	=	conduction current density
k	=	thermal conductivity
$\mathbf{K}$	=	surface electric current density
M	=	Mach number
p	=	pressure
Pr	=	Prandtl number
$\mathbf{q}$	=	heat flux vector
Re	=	Reynolds number
t	=	time
T	=	temperature
T_r	=	reference temperature
u, v, w	=	Cartesian velocity components
x, y, z	=	Cartesian coordinates
ϵ_e	=	dielectric constant in free space
γ	=	ratio of specific heat
μ	=	dynamic viscosity
μ_e	=	magnetic permeability in free space
ρ	=	density of fluid
ρ_e	=	local electric charge density
σ	=	electrical conductivity of fluid
$\bar{\bar{\tau}}$	=	viscous stress tensor

2 Introduction

Sustained hypersonic flights offer potentially revolutionary improvements in space access. Limiting factors

*Graduate Student, Mechanical and Aerospace Engineering Department.

†Associate Professor, Mechanical and Aerospace Engineering Department, Associate Fellow, AIAA.

‡Senior Engineer, Associate Fellow, AIAA.

§Air Vehicles Directorate, Senior Research Engineer, Associate Fellow, AIAA.

in hypersonic vehicle performance include aerodynamic drag and heating rates exerted on the vehicles by surrounding flow fields. Recent research has indicated that hypersonic flow fields may be modified significantly by magnetic Lorentz forces through the creation and manipulation of plasma near the vehicles [1]. Such concepts can be used to control hypersonic flows by suppressing or enhancing hypersonic boundary-layer instability and transition. The suppression of the onset of hypersonic boundary layer transition can lead to significant drag and heating reductions. MHD control of hypersonic boundary layer transition presents a challenge which requires both an understanding of the complex hypersonic MHD flow physics involving the stability and transition of boundary layer. Currently, there have not been many studies on MHD effects on supersonic and hypersonic boundary layer stability and transition. Such MHD effects cannot not be analyzed by the popular linear stability analysis (LST) for supersonic boundary layers because the MHD effects can alter the mean flow profiles substantially so that the parallel flow assumption used in LST is no longer valid.

2.1 MHD Effects on Weakly Ionized Hypersonic Flows

In hypersonic flow, the gas can become weakly ionized either by viscous heating or by artificially generated plasma in the flow. If there is an imposed electromagnetic field in the flow, the flow properties can be changed substantially by the interaction of the electrically conducting gas and the electromagnetic field. Such interaction forms the basic idea of the electromagnetic control of hypersonic flow. Many researchers have shown that hypersonic flow can be altered significantly by Lorentz force [2–8]. It was found that MHD effects weaken the bow shock structure and significantly reduce shock standoff distance for hypersonic flow over a blunt body with the presence of an imposed magnetic field.

Rossow [9] first studied the incompressible boundary layer flow over a flat plate in the presence of a uniform magnetic field applied normal to the plate. The electrical conductivity was assumed to be constant. The MHD boundary-layer equations were solved by numerical integration. He found that the skin friction and heat transfer rates were reduced when the transverse magnetic field was fixed to the plate, but increased when the magnetic field was fixed to the moving fluid. In both cases, the total drag was found to be increased. Bleviss [10] investigated MHD effects on hypersonic Couette flow in which a uniform magnetic field normal to the wall was externally imposed. Assuming variations of electrical conductivity, viscosity, and Prandtl number with temperature, the flow was solved exactly with minimum assumptions about the gas. The results for the case of thermally insulated wall showed a tremendous decrease in skin friction and significant increase in total drag with reasonable magnetic field strength. It was also found that the temperature increased across the flow field and heat transfer increased at the moving wall. For the heat transfer case, a significant increase in total drag was accompanied by a moderate increase in the heat transfer. The interesting result however, was the hysteresis character of the skin friction which was absent in the case of the thermally insulated wall. Bleviss attributed the hysteresis behavior to the dramatic variation of the electrical conductivity with enthalpy that was present in the heat transfer case. Due to the fact that pure shear flow contained many important features of boundary layer flow, Bleviss expected that the magnetic field would decrease the heat transfer and the skin friction but increase the total drag. Furthermore, the hysteresis effect was expected to be present in boundary layer flow. In 1960, Bush [11] studied a high-speed compressible air flow over a flat plate under an applied magnetic field having its component normal to the plate proportional to $\frac{1}{\sqrt{x}}$. Variation of electrical conductivity was also considered. In attempt to verify Bleviss's predictions on boundary layer flow, Bush found that the skin friction and heat transfer decreased with increasing magnetic field strength. Moreover, the boundary layer flow also exhibited the hysteresis behavior as found in the case of MHD Couette flow, but disappeared at much higher Mach number.

Since the magnetic field applied to hypersonic flow can modify the flow field significantly, it is expected that there are strong effects of magnetic field on the stability and transition of supersonic boundary layers. Effects of MHD on boundary-layer stability were investigated by Rossow [12] using a linear stability analysis. The effectiveness of a magnetic field in stabilizing the laminar flow of an incompressible, electrically conducting fluid was studied. A two-dimensional infinitesimal sinusoidal disturbance of a given wave number was impressed on the fluid to test for the stability of the flow in the presence of either a coplanar or transverse magnetic field. Rossow obtained the neutral stability curve and found that the flow over a flat plate was stabilized by either a coplanar or transverse magnetic field fixed relative to the plate, but destabilized when the transverse magnetic field was fixed relative to the fluid. He attributed the destabilizing effect to the inherently unstable velocity profile induced by the magnetic field.

2.2 Supersonic Boundary Layer Instability

The transition process in boundary layers is the result of the nonlinear response of the laminar boundary layers to forcing disturbances [13]. In an environment with small initial disturbances corresponding to those encountered in hypersonic flights, the paths to transition consist of three stages: 1) receptivity, 2) linear eigenmode growth or transient growth, and 3) nonlinear breakdown to turbulence. The process of instability and transition is much more complex and much less under-

stood for hypersonic boundary layers than for low-speed incompressible boundary layers. Most of our knowledge on the stability properties of hypersonic boundary layers is obtained by the analyses of local parallel linear stability theory (LST) [14,15]. Lees and Lin [16] showed that the existence of a generalized inflection point is a necessary condition for inviscid instability of a compressible boundary layer. Mack [14] found that there are higher acoustic instability modes in addition to the first-mode instability waves in supersonic and hypersonic boundary layers. Among them, the second mode becomes the dominant instability for hypersonic boundary layers at Mach numbers larger than about 4. The existence and dominance of the second mode have been validated by experimental stability studies [17]. The second mode has been found to be most unstable when two-dimensional. Currently, it is not known how an imposed magnetic field will affect the stability characteristics of the second mode. This is the focus of the study presented in this paper.

2.3 DNS of Supersonic Boundary Layer Instability

Due to the difficulty in conducting ground-based hypervelocity experiments and the complexity of hypersonic flows, the approach of direct numerical simulation without empirical turbulence models is a potentially powerful tool in studying and understanding supersonic and hypersonic flow physics for the development of future hypersonic space vehicles. In DNS studies, the full unsteady Navier-Stokes equations are numerically simulated without using any empirical turbulence models. The development of instability waves and nonlinear breakdown are numerically captured by the simulation. Though such a simulation is computationally intensive, it has the ability to simulate many of the effects that are neglected by parallel linear stability theory (LST) and parabolic stability equations (PSE) [18].

Erlebacher et al. [19,20] studied the secondary instability mechanism of compressible boundary layers over a flat plate by temporal and spatial direct numerical simulation. Thumm et al. [21], Fasel et al. [22], and Eibler et al. [23,24] performed spatial DNS of the oblique breakdown of transition in a supersonic boundary layer over a flat plate based on compressible 3-D Navier-Stokes equations. Adams and Kleiser [25,26] studied the subharmonic transition process of a flat-plate at a freestream Mach number of 4.5 by temporal direct numerical simulation. Pruett et al. [27–29] performed spatial simulations for supersonic boundary layers over flat plates and sharp cones. The results are compared with parabolic stability equations (PSE). All these DNS studies on compressible boundary layers show that the DNS of high-speed boundary layer transition is feasible on existing computers using efficient and accurate numerical methods. They can provide detailed information which can not be obtained by other means for the study of transition of hypersonic boundary layers.

In the past several years, Zhong and his colleagues at UCLA have been developing new fifth and higher order DNS methods and computer codes for the DNS studies of supersonic and hypersonic boundary layer stability and transition in non-trivial geometries with bow shock effects [30]. We have also conducted DNS studies of the receptivity and stability of a number of 2-D and 3-D hypersonic flows over blunt bodies [31]. The direct numerical simulation as well as other supporting theoretical approaches are used to gain a fundamental understanding of the physical mechanism of laminar-turbulent transition of hypersonic boundary layers over complex 3-D maneuvering vehicles affected by shock waves and real-gas effects. The numerical tools developed in these studies are extended to the current study of MHD effects of the second mode instability.

2.4 Scope of Current Study

The study by Rossow was done before the discovery of the second instability mode in supersonic boundary layers by Mack [14]. It has been generally recognized that the second mode is the most dangerous mode in high Mach number boundary layers. So far, the MHD effects on the second mode instability have not been studied. Therefore, the objective of this paper is to investigate MHD effects on the stability of a Mach 4.5 boundary layer by using the approach of direct numerical simulation (DNS). This paper presents the results of a direct numerical simulation on the effects of imposed magnetic field on the propagation of second mode instability in a Mach 4.5 boundary layer. The two-dimensional steady base flow and unsteady flow are solved by nonlinear Navier-Stokes equations with an imposed magnetic field. The effects of the imposed magnetic field on the second mode instability in the supersonic boundary layer are investigated by the numerical simulations. These results represent the first of this kind in demonstrating the properties of the second mode under various imposed magnetic fields.

DNS approach is chosen because LST may not apply on the highly nonparallel mean flow distorted by the applied magnetic field. The geometry of this study is rather simple. A Mach 4.5 flow over a two-dimensional flat plate in the presence of an imposed magnetic field is simulated. All vector components and variations of flow properties in the spanwise direction are neglected. The gas is assumed to have constant electrical conductivity of 100 mho/m. The imposed magnetic field is generated by placing two-dimensional magnetic dipoles below the flat plate. The resultant magnetic field is similar to that produced by an array of permanent magnets placed beneath the plate. The governing equations of the MHD flow are formulated from the Navier-Stokes and the Maxwell equations, and are spatially discretized by our fifth-order numerical scheme. In an attempt to

solve the coupled MHD equations, difficulties were encountered due to the constraint of the size of time step posed by the magnetic diffusivity of the magnetic induction equation. To resolve the "stiffness" problem, we solve the approximate MHD equations without the induction equation by neglecting the induced magnetic field and assuming that the imposed magnetic field is constant. This is actually a fair assumption considering that the magnetic Reynolds number is in the order of 10^{-3}. The mean flow and stability analysis of this flow without MHD effects have been studied by Ma and Zhong [32]. The physical domain of the flat plate in this paper corresponds to the region in which the second mode disturbance is the dominant unstable mode. By introducing the second mode disturbance at the entrance on the converged steady flow, we have conducted a series of cases with different configurations of the imposed magnetic fields and investigated the influences of MHD on the second mode instability.

3 Governing Equations

The governing equations of MHD of compressible flow are the Maxwell equations coupled with the Navier-Stokes equations through the momentum and energy equations. In most practical situations, the fluid satisfies the magnetogasdynamic approximations [33] so that the displacement current and the excess electric charge are neglected. The simplified Maxwell equations that apply to MHD are:

$$\nabla \times \frac{\mathbf{B}}{\mu_e} = \mathbf{J} \tag{1}$$

$$\nabla \times \mathbf{E} = -\frac{\partial \mathbf{B}}{\partial \mathbf{t}} \tag{2}$$

$$\nabla \cdot \mathbf{B} = 0 \tag{3}$$

$$\nabla \cdot \mathbf{E} = 0 \tag{4}$$

In Eq (1) and (4), the displacement current $\frac{\partial \epsilon_e \mathbf{E}}{\partial t}$ and the local charge density $\frac{\rho_e}{\epsilon_e}$ are neglected respectively. It implies that the plasma or fluid has the tendency toward electrical neutrality, but this is true only when the Debye length is much smaller than the typical length scale of the flow. The magnetic permeability μ_e that appears in Eq (1) is assumed constant throughout the paper, its value is taken as the same as that in vacuum.

The current density $\mathbf{J}$ in MHD is given by the generalized Ohm's law as follows,

$$\mathbf{J} = \sigma(\mathbf{E} + \mathbf{u} \times \mathbf{B}) \tag{5}$$

where σ is the electrical conductivity. This equation relates the current density with the electric field and the induced electric field generated by crossing the magnetic field lines with the velocity vector. This form of the electric current equation neglects the Hall current for simplicity.

The complete set of MHD equations consists of the continuity equation, momentum equation, magnetic induction equation, and energy equation. The continuity equation has exactly the same form as it appears in the Navier-Stokes equations. The momentum equation is modified by adding the Lorentz force term $\mathbf{J} \times \mathbf{B}$ as a body force, and the energy equation is modified by adding the magnetic energy term $\mathbf{E} \cdot \mathbf{J}$. The magnetic induction equation is obtained by substituting Eq (1) and Eq (5) into Eq (2). It is a vector equation coupled with the velocity vector. It is written as

$$\frac{\partial \mathbf{B}}{\partial t} - \nabla \times (\mathbf{u} \times \mathbf{B}) = \frac{1}{\mu_e \sigma} \nabla^2 \mathbf{B} \tag{6}$$

where $\frac{1}{\mu_e \sigma}$ is the magnetic diffusivity or viscosity. The equation has a very similar form as the vorticity equation in conventional fluid mechanics. It can also be shown that the magnetic field shares many physical phenomena with the vorticity vector. The term on the right hand side of the equation represents diffusion of magnetic field, and under the flow conditions in this paper, the magnitude of the magnetic viscosity is several orders higher than the fluid viscosity. Therefore, it causes a stiffness problem that significantly reduces the size of time step of our simulation. In order to solve the MHD equations more efficiently, we only consider the cases where the small magnetic Reynolds number assumption applies. The magnetic Reynolds number defined as $UL\sigma\mu_e$ is on the order of 10^{-3} for all cases presented in this paper. Since it is much less than unity, we assume that the induced magnetic field is negligible and the imposed magnetic field is constant throughout the computations.

The set of MHD equations with the assumption of negligible induced magnetic field are written as follows:

$$\frac{\partial \rho}{\partial t} + \nabla \cdot (\rho \mathbf{u}) = 0 \tag{7}$$

$$\rho\left(\frac{\partial \mathbf{u}}{\partial t} + \mathbf{u} \cdot \nabla \mathbf{u}\right) = -\nabla p + \nabla \cdot \bar{\bar{\tau}} + \sigma(\mathbf{E} \times \mathbf{B}) + \sigma(\mathbf{u} \times \mathbf{B}) \times \mathbf{B} \tag{8}$$

$$\frac{\partial e}{\partial t} + \nabla \cdot (e\mathbf{u}) = -\nabla \cdot (p\mathbf{u}) + \nabla \cdot (\mathbf{u} \cdot \bar{\bar{\tau}}) - \nabla \cdot \mathbf{q} + \mathbf{E} \cdot \mathbf{J} \tag{9}$$

where $e = \frac{p}{(\gamma-1)} + \frac{1}{2}\rho U^2$, is the internal energy plus the kinetic energy of the fluid. The viscous stress and the heat flux are given by the usual constitutive equations in Newtonian fluid as follows

$$\tau_{ij} = \mu\left(\frac{\partial u_i}{\partial x_j} + \frac{\partial u_j}{\partial x_i}\right) - \frac{2}{3}\mu \frac{\partial u_k}{\partial x_k}\delta_{ij} \tag{10}$$

$$q_i = -k\frac{\partial T}{\partial x_i} \tag{11}$$

where μ is the viscosity coefficient determined by the Sutherland law,

$$\mu = \mu_r \left(\frac{T}{T_r}\right)^{\frac{3}{2}} \frac{T_r + T_s}{T + T_s} \tag{12}$$

where $T_r = 288K$, $T_s = 110K$, and $\mu_r = 0.17894 \times 10^{-4} kg/(ms)$ for air. The thermal conductivity k is computed from the Prandtl number, which is assumed constant and it takes the value of 0.72 in this paper.

The imposed magnetic field in this paper is generated by placing two-dimensional magnetic dipoles below the flat plate. The resultant magnetic field at each point in the flow field is computed by superimposing the magnetic field components induced by each 2-D magnetic dipole. The formula of a 2-D magnetic dipole located at the origin of the coordinate system and pointing up vertically is written as follows

$$\mathbf{B} = \frac{B_0}{r^2}[\sin 2\theta \ \hat{i} - (\cos^2\theta - \sin^2\theta) \ \hat{j}] \qquad (13)$$

where it is assumed that x and y form an orthogonal coordinate system. The magnetic dipole is located at the origin and is pointing in the positive y-direction. θ is the angle measured from the dipole moment (y-axis in this case) to the position vector $\mathbf{r}$, r is the magnitude of the position vector, and B_0 represents the strength of the magnetic dipole. The formulas for other dipoles pointing to other directions can also be derived similarly.

4 Numerical Method

There have been several recent works on developing upwind schemes for MHD equations with shock capturing capability [34,35]. Most of these methods are second-order accurate TVD schemes, which may not be accurate enough for the numerical simulation of instability waves in hypersonic boundary layer. Such simulation requires high-order numerical accuracy in order to capture a wide range of time and length scales in the wave fields. Since our goal is to analyze the stability of supersonic boundary layers with MHD effects, it is necessary to use a high-order and robust numerical scheme for the numerical simulation. Therefore, we use a fifth-order finite difference scheme that we have developed and validated for solving the full Navier-Stokes equation for spatial discretization of the MHD equations [30]. The numerical method used in the current study is briefly summerized in this section. More details on the method and its validations can be found in [30].

In the numerical simulation, the MHD equations (7) to (9) are written in the following conservative form,

$$\frac{\partial U}{\partial t} + \frac{\partial E}{\partial x} + \frac{\partial F}{\partial y} + \frac{\partial G}{\partial z} + \frac{\partial E_v}{\partial x} + \frac{\partial F_v}{\partial y} + \frac{\partial G_v}{\partial z} = M \qquad (14)$$

where U is the solution vector given by

$$U = \{\rho, \rho u, \rho v, \rho w, e\} \qquad (15)$$

E, F, G are the inviscid flux terms, and E_v, F_v, G_v are the viscous terms. M is the MHD source term. They are written as follows

$$E = \begin{Bmatrix} \rho u \\ \rho u^2 + p \\ \rho uv \\ \rho uw \\ (e+p)u \end{Bmatrix} \qquad (16)$$

$$F = \begin{Bmatrix} \rho v \\ \rho uv \\ \rho v^2 + p \\ \rho vw \\ (e+p)v \end{Bmatrix} \qquad (17)$$

$$G = \begin{Bmatrix} \rho w \\ \rho uw \\ \rho vw \\ \rho w^2 + p \\ (e+p)w \end{Bmatrix} \qquad (18)$$

$$E_v = -\begin{Bmatrix} 0 \\ \tau_{xx} \\ \tau_{yx} \\ \tau_{zx} \\ u\tau_{xx} + v\tau_{yx} + w\tau_{zx} - q_x \end{Bmatrix} \qquad (19)$$

$$F_v = -\begin{Bmatrix} 0 \\ \tau_{xy} \\ \tau_{yy} \\ \tau_{zy} \\ u\tau_{xy} + v\tau_{yy} + w\tau_{zy} - q_y \end{Bmatrix} \qquad (20)$$

$$G_v = -\begin{Bmatrix} 0 \\ \tau_{xz} \\ \tau_{yz} \\ \tau_{zz} \\ u\tau_{zx} + v\tau_{zy} + w\tau_{zz} - q_z \end{Bmatrix} \qquad (21)$$

$$M = \sigma\begin{Bmatrix} 0 \\ -u({B_y}^2 + {B_z}^2) + vB_xB_y + wB_xB_z \\ uB_xB_y - v({B_x}^2 + {B_z}^2) + wB_yBz \\ uB_xB_z + vB_yB_z - w({B_x}^2 + {B_y}^2) \\ 0 \end{Bmatrix} \qquad (22)$$

In the conservation equation (14), the inviscid fluxes and the viscous fluxes have the same forms as those of the Navier-Stokes equations. The new term, M, represents the contribution of the Lorentz force $\mathbf{J} \times \mathbf{B}$. In this paper, the imposed electric field is assumed to be zero for simplicity.

Before discretizing the governing equation by a finite difference method, equation (14) in the physical domain is transformed to the body-fitted computational domain by the following transformation relations,

$$\begin{cases} \xi = \xi(x,y,z) \\ \eta = \eta(x,y,z,t) \\ \zeta = \zeta(x,y,z) \\ \tau = t \end{cases} \iff \begin{cases} x = x(\xi,\eta,\zeta,\tau) \\ y = y(\xi,\eta,\zeta,\tau) \\ y = y(\xi,\eta,\zeta,\tau) \\ t = \tau \end{cases} \qquad (23)$$

and the transformed governing equation in the compu-

tational domain is expressed as follows

$$\frac{1}{J}\frac{\partial U}{\partial \tau}+\frac{\partial E'}{\partial \xi}+\frac{\partial F'}{\partial \eta}+\frac{\partial G'}{\partial \zeta} +\frac{\partial E'_v}{\partial \xi}+\frac{\partial F'_v}{\partial \eta}+\frac{\partial G'_v}{\partial \zeta}+U\frac{\partial(\frac{1}{J})}{\partial \tau}=M \tag{24}$$

A fifth-order explicit finite difference scheme is used for spatial discretization of the governing equation (24), the inviscid flux terms are discretized by the upwind scheme, and the viscous flux terms are discretized by the central scheme. For the inviscid flux vectors, the flux Jacobians contain both positive and negative eigenvalues, a simple local Lax-Friedrichs scheme is used to split the inviscid flux vectors into positive and negative wave fields. For example, the flux term F' in Eq (24) can be split into two terms of pure positive and negative eigenvalues as follows

$$F' = F'_+ + F'_- \tag{25}$$

where $F'_+ = \frac{1}{2}(F' + \lambda U)$ and $F'_- = \frac{1}{2}(F' - \lambda U)$ and λ is chosen to be larger than the local maximum eigenvalue of F'

$$\lambda = \frac{|\nabla \eta|}{J}\left(\sqrt{(\epsilon c)^2 + u'^2} + c\right) \tag{26}$$

where

$$u' = \frac{\eta_x u + \eta_y v + \eta_z w + \eta_t}{|\nabla \eta|} \tag{27}$$

The parameter ϵ is a small positive constant added to adjust the smoothness of the splitting. The fluxes F'_+ and F'_- contain only positive and negative eigenvalues respectively. Therefore, in the spatial discretization of equation (24), the derivative of the flux F is split into two terms

$$\frac{\partial F'}{\partial \eta} = \frac{\partial F'_+}{\partial \eta} + \frac{\partial F'_-}{\partial \eta} \tag{28}$$

where the first term on the right hand side is discretized by the upwind scheme and the second term by the downwind scheme.

The fifth-order explicit scheme utilizes a 7-point stencil and has a adjustable parameter α as follows

$$u'_i = \frac{1}{h\, b_i}\sum_{k=-3}^{3} a_{i+k}\, u_{i+k} - \frac{\alpha}{6!\, b_i} h^5 \left(\frac{\partial u^6}{\partial^6 x}\right)_i + \cdots \tag{29}$$

where $a_{i\pm 3} = \pm 1 + \frac{1}{12}\alpha$, $a_{i\pm 2} = \mp 9 - \frac{1}{2}\alpha$, $a_{i\pm 1} = \pm 45 + \frac{5}{4}\alpha$, $a_i = 0 - \frac{5}{3}\alpha$, and $b_i = 60$. The scheme is upwind when $\alpha < 0$ and downwind when $\alpha > 0$. It becomes a sixth-order central scheme when $\alpha = 0$.

5 Boundary Conditions

The computational domain is weakly ionized supersonic flow over a flat plate with an imposed magnetic field. A schematic of the flow field with an imposed magnetic field is shown in Figure 1. The flow direction is from left to right. The upper boundary of the computational domain is a weak oblique shock induced by boundary layer thickness. The boundary conditions are described below.

5.1 Upper Boundary

The attached weak shock that originates from the leading edge of the flat plate serves as the upper computational boundary in the numerical simulation. The location of the shock is determined by a shock fitting method [30]. The flow variables behind the shock are determined by the Rankine Hugoniot relation across the shock and a characteristic compatibility equation behind the shock. The MHD terms are not taken into account in the Rankine Hugoniot relation because the magnetic field strength considered is mainly concentrated near the wall and the magnetic field strength at the upper boundary is approximately less than 5 percent of the maximum value at the wall. In addition, because the shock is very weak and far away from the boundary layer, it plays no role in the second mode propagation in the boundary layer. Therefore, we assume that the local magnetic field at the shock is too weak to alter the shock location significantly.

It should be noted that such assumption may not be appropriate for flow across a strong bow shock in the nose region of hypersonic and high-temperature flow over a blunt body. The magnetic field in the local region at the shock can be strong and the local electrical conductivity can be large there. In those cases, it is necessary to include the B field effects in the shock fitting formulas.

5.2 Lower Boundary

The flat plate itself is the lower computational boundary, it is assumed to be adiabatic so that $\frac{\partial T}{\partial y} = 0$ is enforced at the wall. The velocity components u and w are zero following the non-slip wall condition and v is zero according to the solid-wall condition. For the magnetic field lines across the lower boundary, the normal component of the magnetic field across the flat plate is continuous. The flat plate is assumed non-magnetic such that the tangential component across the boundary is given by

$$\hat{\mathbf{n}} \times (\mathbf{B_2} - \mathbf{B_1}) = \mu_e \mathbf{K} \tag{30}$$

where $\hat{\mathbf{n}}$ is the surface normal vector and $\mathbf{K}$ is the surface current density. We assume that the flat plate is electrically insulated, therefore the surface current density is zero and the tangential component of the magnetic field is continuous across the flat plate.

5.3 Inlet and Exit Conditions

The inlet conditions are fixed and are given by the initial conditions of the flow. The flow variables at the exit are extrapolated from the interior points as done in [30].

6 Flow Conditions

In this paper, Mach 4.5 weakly ionized viscous flows over a flat plate in various imposed magnetic fields are considered. The flow conditions in all cases are the same except the magnetic fields. They are: $M_\infty = 4.5$, $T_\infty = 65.15\ K$, $p = 728.438\ Pa$, $Pr = 0.72$, $Re_\infty = 7.2 \times 10^6/m$, and $\sigma = 100\ mho/m$. The focus of the study is on the MHD effects on the stability of second mode wave disturbances. The steady flow solution and the second mode stability of the same flow without MHD effects have been studied by direct numerical simulation by Ma and Zhong [32]. The velocity vectors shown in the schematic of the flow with imposed magnetic field in Figure 1 are those computed without the imposed magnetic field. The steady flow solution for the case without MHD effects of Ma and Zhong [32] is used as the basis for evaluating the MHD case. In addition, the numerical accuracy of the results have been extensively validated in the previous work [32].

In the current simulation, the flat plate has a length of $0.048m$. The physical domain is resolved by 240 uniform grids in the horizontal direction and 120 stretched grids in the vertical direction. A total of seven different imposed magnetic fields are considered to investigate the effects of magnetic field orientations, where the imposed magnetic field of each case is calculated by the superposition of the magnetic dipoles located below the plate. The schematic of the flow with imposed magnetic field is shown in Figure 1.

The solutions include both steady solutions and unsteady solutions with second mode instability waves propagating in the boundary layers. The effects of the imposed magnetic fields on both steady and unsteady solutions are investigated. The results of these numerical studies are presented in the following sections.

7 MHD Effects on Steady Flow Solutions

The effects of an imposed magnetic field on steady supersonic boundary-layer flow over a flat plate are first studied. The magnetic fields are generated by placing several magnetic dipoles under the plate. Six cases of different dipole arrangements, in terms of orientations and spacing of the dipoles, are considered to better understand the MHD effects on supersonic flow.

7.1 Case I. A Pair of Dipoles Pointing Vertically in the Opposite Directions

We first consider the case of Mach 4.5 flow over a flat plate with two magnetic dipoles of equal strength, one pointing vertically upward and another downward. The centers of two dipoles are located below the flat plate. The first dipole is located at a distance of $0.02m$ from the inlet and $0.01m$ below the plate. Its dipole moment is pointing in the positive y-direction. The second dipole is located at a distance of $0.025m$ from the inlet, and has the same y-location as the first one. The dipole moment of the second dipole is pointing in the negative y-direction. For this magnetic dipole arrangement, two sub-cases of different magnetic field strength are considered, i.e.,

Case I.a: Relatively weak B-field of $B_0 = 1.5 \times 10^{-4} Tm^2$,
Case I.b: Relatively strong B-field of $B_0 = 3 \times 10^{-4} Tm^2$.

where B_0 is the magnitude in equation (13). The value of B_0 is chosen such that the maximum strength of Case I.b with stronger B-field is about 2.5 T on the wall and that for Case I.a of weaker one is about 1.2 T on the wall.

Figure 2 shows the magnetic field lines and the contours of the B-field magnitude for the case of weaker B-field. The B-field distributions for the case of stronger magnetic field are similar to these plots except that the magnitude is twice as strong for the latter case. The figure shows that the magnetic field strength is mainly concentrated in the boundary layer region near the plate surface. It is expected that it will have the strongest effect on the boundary layer structure near the wall.

Numerical results of steady Mach 4.5 weakly ionized flow with a pair of dipoles for both cases of $B_0 = 1.5 \times 10^{-4} Tm^2$ and $B_0 = 3 \times 10^{-4} Tm^2$ are obtained by using a fifth order scheme. The results are shown in Figures 3 to 9. In general, the MHD effects on the steady flow by the strong and weak magnetic fields have very similar trends. The strong B-field alters the flow significantly while the weak B-field modifies the flow in a relatively lesser degree. Figure 3 compares the velocity profiles affected by the imposed magnetic fields for the cases of $B_0 = 1.5 \times 10^{-4} Tm^2$ and $B_0 = 3 \times 10^{-4} Tm^2$. This figure shows that the flow in the vicinity of the boundary layer is retarded by the opposing Lorentz force, this also results in the thickening of the boundary layer. It is observed that the magnetic fields induce strong modifications on the vertical velocity components. The magnetic effects on the velocity fields are similar for both cases except that they appear to be much stronger in the stronger B-field case.

The contours of flow variables for the cases of weaker and stronger magnetic fields and the case of no magnetic field are shown in figures 4, 5, and 6. From the contours of normal velocity and pressure, it is observed that the magnetic forces induce a new shock structure outside of the boundary layer. It is identified as the Mach wave associated with the interaction of the flow with the Lorentz force, since the angle between the new shock and the flat plate is approximately equal to the Mach angle. Comparing the new shocks in both cases,

the new shock in the stronger field case is much sharper while it is relatively smeared in the weak field case, it indicates that the stronger magnetic field produces a much stronger Mach wave. The normalized pressure on the wall and the skin friction coefficient are shown in Figure 7 and 8 respectively. The magnetic dipoles introduce adverse pressure gradient on certain regions but favorable pressure gradient on other regions. The skin friction coefficient is found to be reduced everywhere on the flat plate for both cases. For the case of strong magnetic field, the local adverse pressure gradient is sufficient to cause local flow separation. There is a local region on the wall where negative skin friction is produced by the magnetic field, which is an indication of a local separation region. The local separation bubble, which can be demonstrated by streamlines shown in figure 9, is found near the inlet. It is due to the relatively strong adverse pressure gradient in that region.

Due to the local separation created by the imposed magnetic field, the smooth development of the supersonic boundary layer has been changed. It is natural to expect that the flow will become more unstable, and it is interesting to investigate how the characteristics of the boundary-layer instability modes, especially the second mode, are affected by the magnetic field. It will be shown later that contrary to intuitive expectation, the second mode is substantially disrupted and stabilized by the imposed magnetic field, even though there exists a local separation area.

7.2 Case II. A Pair of Dipoles Pointing Vertically in the Same Direction

In this case, two magnetic dipoles with both of their dipole moments pointing in the positive y-direction is considered. The first magnetic dipole is located at a distance of $0.02m$ from the inlet and $-0.007m$ below of the plate. The second one is located at a distance of $0.025m$ from the inlet, and has the same y-location as the first one. Both dipoles have magnetic field strength specified by $B_0 = 0.45 \times 10^{-4} Tm^2$. The value of B_0 is chosen so that the maximum B field strength is about the same as that of the weaker B-field case of Case I. The magnetic field lines and the magnitude of the B-field are shown in figure 10. Again, the magnetic field is mainly concentrated in the boundary layer on the surface.

Figure 11 shows the steady flow solution in this case. Again, the streamwise velocity is retarded by the B-field and a strong adverse pressure gradient region is generated on the surface. The steady flow variables in this case exhibit very similar behaviors as Case I with a pair of magnetic dipoles in opposite directions. The only noticeable differences appear in the pressure on the wall and the skin friction coefficient. The pressure on the wall in this case has only peak, where there are two peaks in each of the previous cases. There are also less peaks in the skin friction coefficient distributions of the current case than than those of the previous cases. Overall, the effects are similar.

7.3 Case III. Four Dipoles Pointing Vertically in Alternating Directions

We next consider four magnetic dipoles placed beneath the flat plate with their dipole moments pointing in alternating vertical directions, i.e., the first one points in the positive y-direction, the second one points in the negative y-direction, and so on. The x-locations of the four dipoles from the inlet are $0.01m$, $0.02m$, $0.03m$, and $0.04m$, respectively. They are all located at $0.005m$ below of the plate. Again, the value of B_0 of all dipoles is chosen so that the maximum B-field strength is about the same as that of the weaker B-field case of Case I. All dipoles have magnetic strength specified by $B_0 = 0.27 \times 10^{-4} Tm^2$. The magnetic field and magnitude are shown in Figure 12. The magnetic field strength in this case spreads over the flat more uniformly than that of the two dipoles cases.

The steady solutions of the Mach 4.5 boundary layer with the presence of these four dipoles are shown in Figure 13. The effects of the imposed magnetic field are again similar to the previous two dipoles cases, except that the pressure on the wall and the skin friction coefficient have more peaks.

7.4 Case IV. Four Dipoles Pointing Vertically in the Same Direction

The effects of four magnetic dipoles with all of their dipole moments pointing in the positive y-direction are investigated. All dipoles are placed below of the plate with their x and y locations the same as the previous four dipoles case. All dipoles have a magnetic strength given by $B_0 = 0.37 \times 10^{-4} Tm^2$, which is chosen similar to the previous case. The magnetic field and the magnitude are shown in Figure 14. Again, the magnetic field strength in this case spreads over the flat more uniformly than that in the two dipoles cases.

The steady solutions of Mach 4.5 boundary layer with the presense of these four dipoles are shown in Figure 15. The effects of the imposed magnetic field are again similar to the previous four dipoles cases.

7.5 Case V. A Pair of Dipoles Pointing Horizontally in the Same Direction

The effects of orientation of the dipoles are considered in this case. Two magnetic dipoles with their dipole moments pointing in the positive x-direction are placed below the plate. The first dipole is located at a distance of 0.02 m from the inlet, its y-location is $0.007m$ below of the plate. The second dipole is located at a distance of $0.015m$ from the inlet, and has the same y-location as the first one. All dipoles have a magnetic strength

given by $B_0 = 0.45 \times 10^{-4} Tm^2$, which is chosen similar to the previous case. The magnetic field lines and the magnitude of the resultant magnetic field are shown in Figure 16. The magnetic field for the current case is similar to that of the case of vertical dipoles shown in Figure 2.

Figure 17 shows the steady flow solution in this case. Again, the imposed magnetic field for this case has very similar influence on the steady flow variables as Case I with a pair of vertical dipoles. These results show that the effects of magnetic field on supersonic boundary layers are not very senstive to the orientation of the magnetic dipoles.

7.6 Case VI. Four Dipoles Pointing Horizontally in the Same Direction

Four magnetic dipoles with their dipole moments pointing in the positive x-direction are placed below of the plate. The x-locations of the magnetic dipoles from the inlet are $0.0075m$, $0.0175m$, $0.0275m$, and $0.0375m$, respectively. The y-locations of all of them are $0.005m$ below of the plate. All dipoles have a magnetic strength given by $B_0 = 0.35 \times 10^{-4} Tm^2$, which is chosen similar to the previous case. The magnetic field lines and the magnitude of the resultant magnetic field are shown in Figure 18. The results of steady flow over a flat plate are shown in Figure 19. The flow exhibits similar characteristics as the vertical dipoles cases, but the profiles of the pressure and the skin friction coefficient are quite different in this case.

For all cases considered, the magnetic fields have very similar effects on the supersonic boundary layer. The results show that the flow in the vicinity of the boundary layer is retarded by the opposing Lorentz force. This also results in the thickening of the boundary layer. The magnetic field shows strong modifications on the vertical velocity components for all cases. For the case of very strong B-field, a local separation region is created by the imposed magnetic field.

8 MHD Effects on Second-Mode Instability Waves

The steady flow solutions presented in the previous section show substantial alterations of the boundary layer structure by the imposed magnetic fields. The effects of the magnetic fields on the stability of supersonic boundary layers are investigated in this section. Mack [14] showed that, unlike low speed boundary layers, there are multiple instability modes in supersonic boundary layers. Among these instability modes, the second mode is the most unstable one at high Mach numbers. The second mode waves are most unstable when they are two-dimensional, i.e., they are most unstable when they propagate in the same plane as the mean flow. Therefore, this paper mainly studies the MHD effects on the two-dimensional second mode instability in the supersonic boundary layer. Since the mean flow under the influence of the magnetic field is no longer parallel, the linear stability approach is not expected to be valid. The most effective approach is the DNS study of the propagation of the second mode wave through the supersonic boundary layer with an imposed magnetic field. This is the approach that we adopt in this paper.

In this section, we will first discuss the second mode instability results for Mach 4.5 flow without MHD effects. These results were obtained by Ma and Zhong in [32]. The second mode results without MHD effects are used as bases of comparison on the MHD effects. Subsequently, we will present the results of the propagation of a second mode instability wave passing through the supersonic boundary layer with the same six cases of different arrangements of magnetic dipoles discussed in the preceding section.

8.1 Second-Mode Instability Waves in Supersonic Boundary Layers

Thanks to the work of Mack [14] and many others, it has been generally accepted that the linear stability analysis is very accurate to describe the characteristics of supersonic boundary layer instability (LST) in the linear development region. In a two-dimensional LST study, the disturbances of the unsteady flow in the boundary layer are represented by the perturbations of instantaneous flow variables with respect to their local mean variables, such as

$$u'(x, y, t) = u(x, y, t) - \bar{u}(x, y) \tag{31}$$

where $\bar{u}(x, y)$ is the mean flow velocity. The linear stability analysis decomposes the fluctuations of an arbitrary variable, $\tilde{\mathbf{q}}$ in a normal mode form as follows

$$\tilde{\mathbf{q}} = \hat{\mathbf{q}}(y) e^{(\alpha x - \omega t)} \tag{32}$$

where $\tilde{\mathbf{q}} = \{\tilde{u}, \tilde{v}, \tilde{p}, \tilde{T}, \tilde{w}\}^{tr}$, and $\hat{\mathbf{q}} = \{\hat{u}, \hat{v}, \hat{p}, \hat{T}, \hat{w}\}^{tr}$. $\hat{\mathbf{q}}$ is complex amplitude of the disturbance, $\alpha = \alpha_r + i\alpha_i$, is the streamwise wavenumber and growth rate, and $\omega = \omega^* L / u_\infty$ is the frequency. The frequency of the disturbance is generally characterized by a dimensionless frequency F, defined by $F = \mu / (\rho u^2)_\infty$.

The linear stability analysis uses a local parallel mean flow assumption to derive a linearized governing equation with homogeneous boundary conditions for flow disturbances. The resulting equations form an eigenvalue problem. For the spatial stability problem, ω is a given real parameter while α and $\hat{\mathbf{q}}(y)$, both of which are complex, are solved as eigenvalue and eigenfunction of the linear stability equation. These solutions form various modes of the boundary layer waves. A mode is stable if α_i is nonnegative. Otherwise, it is unstable. For supersonic flow, besides the first mode, Mack found a new family of unstable modes called Mack modes [36].

For the Mach 4.5 boundary layer with MHD effects studied in this paper, the first and second modes neutral curve have been calculated by Ma and Zhong [32] using a multi-domain spectral method presented by Malik [37]. Figure 20 shows the neutral curves of stability (F vs R) for two-dimensional first and second mode disturbances at Mach 4.5. In the figure, the nondimensional parameter R is the local Reynolds number defined using the length scale of boundary layer thickness, i.e.,

$$R = \rho_\infty u_\infty L/\mu_\infty = \sqrt{Re_x} \tag{33}$$

where length scale of boundary layer is defined as

$$L = \sqrt{\frac{\mu_\infty x}{\rho_\infty u_\infty}}. \tag{34}$$

The region inside of the upper dash-dot curve is the second mode instability region, while the region inside of the solid curve is the first-mode instability region. The region outside of these curves is a stable region. The figure shows that the second mode is unstable at high frequency as compared to the first mode.

We chose the linear development of a second mode wave at a fixed frequency in the Mach 4.5 boundary layer. The frequency is $F = 2.2 \times 10^{-4}$ as shown in Figure 20. It is chosen based on the neutral stability curve such that it is unstable in this region in non-MHD flow. The amplitude of the wave is small so that the development of it is essentially linear. The computational domain in the current calculations is inside the second mode instability region in the figure. Therefore, the amplitude of the second mode wave grows as it travels downstream when there are no MHD effects in the flow field. In the numerical simulation, a second mode wave obtained from LST, is introduced at the inlet on the left hand side of the computational domain over the steady flow solution obtained from previous section. The effect on the wave disturbance is then simulated by solving the full Navier-Stokes equations with the MHD effects. The stability results of the second mode propagation without MHD has been studied by Ma and Zhong [32] by numerical simulations. The results are shown in Figure 21. The figure shows the growth of the wave amplitude along the flow direction. The figure also shows the well-known properties of the second mode that the pressure perturbation is concentrated on the wall, but the density and temperature perturbations are largest at the edge of the boundary layer, which forms the so called rope waves observed in experiments [38].

The propagation of second mode instability waves in the boundary layer under the influence of magnetic fields are subsequently studied by direct numerical simulation. The results of second mode instability in all six cases of magnetic field arrangements (Case I to VI) discussed in the previous section are compared with those of second mode wave without MHD effects.

8.2 Case I. A Pair of Dipoles Pointing Vertically in the Opposite Directions

In this case, the stability of the second mode disturbance is investigated under the influence of a pair of magnetic dipoles pointing in opposite directions. The arrangements of the dipoles are given in Case I of the preceding section. Specifically, two cases are considered with a weak field (Case I.a) and strong field (Case I.b). The corresponding steady flow solutions are presented in the preceding section.

Figure 22 shows the results of the second mode disturbances in the boundary layer for Case I.a of a pair of magnetic dipoles in opposite vertical directions of weak magnetic field at $B_0 = 1.5 \times 10^{-4} Tm^2$. Compared with the non-MHD results of Figure 21, the imposed magnetic field has a stabilizing effect on the second mode disturbances. The plots of the instantaneous disturbance of pressure on the wall clearly show that the wave is slightly destabilized in the early zone near the inlet, and then stabilized in the regions where they would be destabilized in the non-MHD case. The disturbance of pressure exhibits a transitional point at about $x = 0.13m$, where the disturbance dies down and gets re-excited before and after that point. The propagation of the second mode wave is substantially damped at $x = 0.13m$, followed by the development of a much weaker wave. The density and temperature contours also show the sudden damping of the second mode wave at $x = 0.13m$.

Similar results are found for Case I.b of the stronger magnetic field as shown in Figure 23. In this case, the stabilization effect on the second mode by the magnetic force is stronger. The second mode wave is significantly stabilized. Again the phase angle distribution shows discontinuous steps at the transitional points, which indicate changes of wave mode. Although the steady flow in this case has a local separation region (Figure 9), the second-mode wave disturbance is still stabilized by the magnetic field. This result was somewhat unexpected since one might expect that the separation bubble would greatly destabilize the boundary layer.

The suppression of the second mode can also be examined by the plots of the Fourier phase angles of the waves. The phase angles are obtained by a temporal Fourier analysis on the numerical solutions of the perturbations of the unsteady flow variables after a periodic state has been reached in a simulation. A Fourier transform of a disturbance variable leads to:

$$q'(x,y,t) = \Re\{|q'(x,y)|\, e^{i[-\omega t + \phi(x,y)]}\} \tag{35}$$

where ω is the forcing frequency of the acoustic wave in the free stream, $q'(x,y,t)$ represents any instantaneous perturbation variables. $|q'(x,y)|$ and $\phi(x,y)$ are the local perturbation amplitude and phase angle respectively. For simulation with small perturbation, only linear responses are significant in the results. $\phi(x,y)$

indicates a local phase angle with respect to the forcing wave in the free stream. If the wave modes in the boundary layer on the body surface are dominated by a single wave mode, $\phi(x, y)$ on the surface should be linear with respect to x, i.e.,

$$\phi(x, 0) = \alpha_r x + \phi_0 \tag{36}$$

where α_r is the wave number. Any discontinuity or step in the distribution of $\phi(x, 0)$ as a function of x represents a change of dominant wave mode in the disturbance, i.e., the decay of one wave mode followed by the growth of another wave mode. Therefore, the $\phi(x, 0)$ distribution can indicate the change of wave mode in the boundary layer.

The plots of the phase angle for the weak and strong field cases are shown in Figure 22 and Figure 23 respectively. In the weak field case, the distribution of the phase angle of the disturbance shows a small discontinuous step between the region of damping of the original second mode and the development of a new wave downstream. In the strong field case, more than one discontinuity of the phase angle is observed. The locations of the discontinuities for both cases roughly correspond to the transitional points that appear on the plots of the instantaneous disturbance of pressure. This is an indication that the waves before and after the step in phase angle are two different wave modes: the original second mode and a new mode afterward.

8.3 Other Cases on Various Magnetic Dipoles Arrangements

The effects of five other cases of magnetic dipoles arrangements, corresponding to Cases II to VI, on the second mode instability are considered. These cases are:

Case II: A pair of dipoles pointing vertically in the same direction.
Case III: Four dipoles pointing vertically in alternating directions.
Case IV: Four dipoles pointing vertically in the same direction.
Case V: A pair of dipoles pointing horizontally in the same direction.
Case VI: Four dipoles pointing horizontally in the same direction.

The steady flow solutions for all these cases are presented in the preceding section.

Figures 24 and 25 show the distributions of the instantaneous surface pressure perturbations for all these cases. All cases have the same flow conditions except that the arrangements and orientations of the magnetic fields are different. In general the magnetic effects on the second mode for all arrangements are very similar to that in Case I.a where the magnetic dipoles point in opposite directions as shown in Figure 22. The second mode wave disturbances are always stabilized by the imposed magnetic fields, after some slight destabilization initially. The wave mode transitional points in the instantaneous pressure distributions correspond to the discontinuities or steps in phase angle distributions. The general trend is that the imposed magnetic field stabilizes the second mode and induces the development of a weaker wave mode afterward.

For Case VI of four magnetic dipoles pointing in the positive x-direction are placed below of the plate, the stabilizing effect on the second mode wave disturbance occurs at further downstream compared with all previous cases. From the plot of instantaneous disturbance of pressure, the second mode is destabilized from the inlet to $x = 0.132m$, this destabilizing region is considerably wider than all those regions in the above cases. Because of the widening of the destabilizing region, the stabilizing effect is delayed and the second mode is not significantly stabilized until the transitional point is reached. The transitional point that corresponds to the discontinuity of the phase angle is located near the exit of the plate. Eventually, the second mode is stabilized by the magnetic field.

The overall effects on the second mode instability by different imposed magnetic fields are compared in Figure 26 and Figure 27. Figure 26 shows the effectiveness of the stabilizing effects on the disturbance by comparing the pressure perturbation amplitudes along the wall of different magnetic field configurations. The solid line in each of the plots is the result of the second mode growth when there is no magnetic field for comparison. The strong magnetic field in the two vertical dipoles case has the most stabilizing effects while the four horizontal dipoles case has the least. For all other cases, the stabilization effects on the second mode are very similar. The amplitudes reach a peak followed by rapid drop of wave amplitudes due to stabilization.

Figure 27 compares the effects of the magnetic field strengths for Case I of the two vertical dipoles on the pressure and temperature disturbance amplitudes. A non-dimensional parameter, $Q = \frac{\sigma B^2 l}{\rho U}$, is used to characterize the magnitude of the Lorentz force over the inertial force, where B is the maximum magnetic field strength on the plate surface. The result in this figure shows that the higher the value of Q, the greater is the stabilizing effect. The common characteristics among the MHD effects on the second mode is that the disturbance is not stabilized until the wave-mode transition of the phase angle takes place.

Figure 28 shows the evolutions of the real part of the eigenfunction of pressure disturbances with and without magnetic field at several grid stations along the flat plate. The imposed magnetic field in this case corresponds to Case I.b of the strong field case of the two vertical magnetic dipoles. As discussed earlier, the wave disturbance undergoes mode shift after the second mode

is stabilized. The mode shift for this case occurs in the region between $x = 0.12m$ and $0.13m$. The figure shows that the mode shape at $x = 0.115m$ before the mode change is substantially different from that of $x = 0.135m$ after the mode change. In plot (c) two distinct bumps appear between $y = 0$ and $y = 0.003m$, one of the bumps however, disappears at later zone ($x = 0.145m$) after another transition of the phase angle has taken place. This suggests that the disturbance tends to undergo mode shift. The evolutions of the wave disturbance in other imposed magnetic fields are found to have similar characteristics as those shown here. They are not presented here due to length limits. Notice in the figure that the shapes of the eigenfunctions at different x go through a gradual change from the profile similar to the first mode to that of a second mode. Such evolution of the eigenfunctions is expected. It is found found that all Mack modes at a fixed frequency, including the first and second modes, are different sections of the same wave mode as it propagates from upstream to downstream.

9 Result Discussions

In this paper, the steady and unsteady results of the Mach 4.5 boundary layer under various magnetic fields have been presented in Section 7 and Section 8. These results are discussed further in this section.

The steady flow results indicate that all the imposed magnetic fields considered in this paper can significantly slowdown the flow in the vicinity of the boundary layer due to the opposing Lorentz force. An adverse pressure gradient is created in some regions and can cause separation of the boundary layer if the magnetic field is strong enough. All cases show similar modifications of the boundary layer thickness by the magnetic forces. As a result of the opposing motion induced by the imposed magnetic field, the streamwise velocity modified by the magnetic field exhibits an inflectional profile that was expected to destabilize the boundary layer and lead to early transition of the flow. However, as shown in Section 8, the result is in contrast to this intuitive expectation. It is found that the imposed magnetic field always has stabilizing effects on the second mode wave disturbance.

The effects of six cases of different arrangements of magnetic fields on the second mode instability are studied by direct numerical simulation. All unsteady results show the same trend on the MHD effects on the second mode instability, that the second mode is significantly stabilized in the boundary layer region where the mean flow boundary layer profile is substantially modified. The suppression of the second mode is followed by the development of different wave modes of much weaker amplitudes. This result is somewhat surprising since the separated mean flow was expected to lead to substantial destabilization of the supersonic boundary layer.

One explanation for the strong suppression of the second mode by magnetic forces in a separated flow is the fact the second mode is a trapped acoustic wave reflecting between the wall and a relative sonic layer in the boundary layer. The second mode instability relies only on the existence of a relative supersonic region in the shear layer and does not require the existence of a generalized inflection point. The most-unstable second-mode frequency is strongly tuned to the boundary layer thickness. In the current case of a supersonic boundary layer with an imposed magnetic field, the mean flow boundary layer is substantially altered, forming a local separation for the case with strong magnetic field as shown in Figures 4 and 5. Because of this, the wave length of the original growing second mode is no longer tuned with the boundary layer thickness. On the other hand, the presence of an unstable first mode relies on the existence of a generalized inflection point in the boundary layer. Therefore the first mode may be more strongly affected by inflectional velocity profiles.

We have done some calculations of the MHD effects on the first mode. It is found that the magnetic field actually amplifies the instability of the first mode, as compared to the effects on the second mode. The first mode is generated in the boundary layer region upstream of the second mode region. We did not focus our efforts on the first mode because the 2-D first mode is more stable than the second mode at a supersonic Mach number and thus less relevant to the laminar-turbulent transition than the second mode. For demonstrating the destabilization of the first mode by magnetic field, we have done numerical simulations of a case of first mode development in the same Mach 4.5 boundary layer with similar magnetic field in terms of arrangement and field strength as Case I.a. Eight vertical magnetic dipoles pointing in alternating directions are evenly spread under a flat plate which is exactly four times as long as the one in the second mode study. The flat plate is divided into four zones of equal length, and the resultant magnetic field in each zone resembles closely the distribution of the magnetic field lines as Case I.a. The maximum magnetic field strength on each zone is approximately $1.2T$. The study of the first mode instability is done on the first of the four zones. The simulations again are to obtain both steady and unsteady solutions. The computational domain has smaller value of x because it appears upstream of the second mode. The nondimensional frequency of the first mode is the same as the second mode case of $F = 2.2 \times 10^{-4}$. Figure 29 shows the results of the first mode disturbance in a Mach 4.5 flow over the first one fourth portion of the flat plate. Two vertical dipoles in opposite directions are located below this region, and the maximum field strength is about $1.2T$ on the wall. The results show that the first mode wave is slightly destabilized by the MHD effects. The adverse pressure gradient destabilizes the first mode.

10 Conclusion

Mach 4.5 weakly ionized flows over a two-dimensional flat plate in the presence of a number of imposed magnetic fields have been studied by DNS. The main focus is on the MHD effects on the instability of second mode wave at high Mach number. The effects of imposed magnetic fields on the second mode disturbances are compared with the results with no magnetic field. Six cases of different arrangements of the imposed magnetic fields have been simulated to obtain both steady and unsteady solutions.

The steady flow results show that all the imposed magnetic fields considered in this paper can significantly decelerate the boundary layer. An adverse pressure gradient is created in some regions and can cause separation of the boundary layer if the magnetic field is strong enough. All cases show similar modifications of the boundary layer thickness by the magnetic forces.

The effects of six cases of different arrangements of magnetic fields on the second mode instability are studied by direct numerical simulation. All unsteady results show the general trend of the MHD effects on the fixed-frequency 2-D second mode instability is that the second mode is substantially stabilized in the region where the mean flow boundary layer is substantially modified, despite the adverse pressure gradient and local separation region in the mean flow. The suppression of the second mode is followed by the development of different wave modes of much weaker amplitudes. The degree of stabilization varies and is mainly determined by the strength of the imposed magnetic field, and it is not very sensitive to the different arrangements of the magnetic dipoles. It should be noted that the input disturbance is a 2-D monochromatic wave. In a more realistic flow, it would be expected that lower frequency disturbances tuned to the thicker MHD boundary layer would be present and would be destabilized. One case of MHD effects on the first mode instability is also studied. The results show that, unlike the second mode, the fixed-frequency 2-D first mode is destabilized under the magnetic field because of the adverse pressure gradient. It is conjectured that the stabilization of the second mode is due to the thickening of the boundary layer, because the most unstable second mode frequency is strongly tuned to the boundary layer thickness. On the other hand, the first mode instability is more closely related to the generalized inflection point, and was amplified in the presence of the decelerated boundary layer profiles.

It should be pointed out that this is an initial study of an idealized case with constant electrical conductivity, neglect of the induced magnetic field, simple arrangements of the magnetic dipoles, and monochromatic, 2-D instability waves. This paper, however, does represent the first DNS study on the interaction of the second mode disturbances with an imposed magnetic field.

Acknowledgements: *This research was supported by the Aeronautical Sciences Division of the Air Force Research Laboratory, Air Vehicles Directorate, Dayton, Ohio under a SBIR Phase I grant. The authors would like to thank Mr. Yanbao Ma in the Mechanical and Aerospace Engineering Department at UCLA for providing LST results used in this study.*

References

[1] Shang, J. S., "An Outlook of CEM Multidisciplinary Applications," *AIAA Paper 99-0336*, 1999.

[2] Canupp, P. W., "The influence of magnetic fields for shock waves and hypersonic flows," *AIAA 2000-2260*, 2000.

[3] Damevin, H., Dietiker, J., and Hoffmann, K. A., "Hypersonic flow computations with magnetic field," *AIAA 2000-0451*, 2000.

[4] Agarwal, R. K. and Augustinus, J., "Numerical simulation of compressible viscous MHD flows for reducing supersonic drag of blunt bodies," *AIAA 99-0601*, 1999.

[5] Hoffmann, K. A., Damevin, H., and Dietiker, J., "Numerical simulation of hypersonic magnetohydrodynamic flows," *AIAA 2000-2259*, 2000.

[6] Poggie, J. and Gaitonde, D. V., "Magnetic control of hypersonic blunt body flow," *AIAA 2000-0452*, 2000.

[7] Gaitonde, D. V., "Development of s solver for 3-D nonideal magnetogasdynamics," *AIAA 99-3601*, 1999.

[8] Shang, J. S., Canupp, P. W., and Gaitonde, D. V., "Computational magneto-aerodynamic hypersonics," *AIAA 99-4903*, 1999.

[9] Rossow, V. J., "On flow of electrically conducting fluids over a flat plate in the presence of a transverse magnetic field," *NACA TN 3971*, 1957.

[10] Bleviss, Z. O., "Magnetogasdynamics of hypersonic Couette flow," *Journal of the Aero/Space Sciences*, Vol. 25 no 10, 1958, pp. 601–615.

[11] Bush, W. B., "Compressible flat-plate boundary-layer flow with an applied magnetic field," *Journal of the Aero/Space Sciences*, Vol. 26, 1960, pp. 49–58.

[12] Rossow, V. J., "Boundary-layer stability diagrams for electrically conducting fluids in the presence of a magnetic field," *NACA TN 4282*, 1958.

[13] Reshotko, E., "Boundary Layer Instability, Transition and Control," *AIAA paper 94-0001*, 1996.

[14] Mack, L. M., "Boundary Layer Linear Stability Theory," *AGARD report, No. 709*, 1984, pp. 3–1 to 3–81.

[15] Malik, M. R., "Prediction and Control of Transition in Hypersonic Boundary Layers," *AIAA Paper 87-1414*, June 1987.

[16] Lees, L. and Lin, C. C., "Investigation of the Stability of the Laminar Boundary Layer in Compressible Fluid," *NACA TN No. 1115*, 1946.

[17] Stetson, K. F. and Kimmel, R. L., "On Hypersonic Boundary Layer Stability," *AIAA paper 92-0737*, 1992.

[18] Herbert, T., "Parabolized Stability Equations," *In Progress in Transition Modeling, AGARD-FDP-VKI Special Course*, 1993.

[19] Erlebacher, G. and Hussaini, M. Y., "Numerical Experiments in Supersonic Boundary-Layer Stability," *Physics of Fluids: A*, Vol. 2, 1990, pp. 94–104.

[20] Ng, L. L. and Erlebacher, G., "Secondary Instability in Compressible Boundary Layers," *Physics of Fluids: A*, Vol. 4, 1992, pp. 710–717.

[21] Thumm, A., Wolz, W., and Fasel, H., "Numerical Simulation of Spatially Growing Three-Dimensional Disturbance Waves in Compressible Boundary Layers," *Laminar-Turbulent Transition, IUTAM Symposium, Toulouse, France, 1989*, edited by D. Arnal and R. Michel, Springer-Verlag Berlin, 1990, pp. 303–310.

[22] Fasel, H., Trumm, A., and Bestek, H., "Direct Numerical Simulation of Transition in Supersonic Boundary Layer: Oblique Breakdown," *Transitional and Turbulent Compressible Flows, ASME FED-Vol. 151*, 1993, pp. 77–92.

[23] Eibler, W. and Bestek, H., "Spatial Numerical Simulations for Nonlinear Transition Phenomena in Supersonic Boundary Layers," *Transitional and Turbulent Compressible Flows*, Vol. L. D. Kral and T. A. Zang, editors, pp. 69-76, FED-Vol. 151, ASME, 1993.

[24] Eibler, W. and Bestek, H., "Spatial Numerical Simulations of Linear and Weakly Nonlinear Instabilities in Supersonic Boundary Layers," *Theoretical and Computational Fluid Dynamics*, Vol. 8, 1996, pp. 219–235.

[25] Adams, N. A. and Kleiser, L., "Numerical Simulation of Transition in a Compressible Flat Plate Boundary Layer," *Transitional and Turbulent Compressible Flows, ASME FED-Vol. 151*, 1993, pp. 101–110.

[26] Adams, N. A., "Subharmonic Transition to Turbulence in a Flat-Plate Boundary Layer at Mach Number 4.5," *Journal of Fluid Mechanics*, Vol. 317, 1996, pp. 301–335.

[27] Pruett, C. D. and Chang, C. L., "A Comparison of PSE and DNS for High-Speed Boundary-Layer Flows," *Transitional and Turbulent Compressible Flows*, Vol. L. D. Kral and T. A. Zang, editors, pp. 57-67, FED-Vol. 151, ASME, 1993.

[28] Pruett, C. D., Zang, T. A., Chang, C.-L., and Carpenter, M. H., "Spatial Direct Numerical Simulation of High-Speed Boundary-Layer Flows, Part I: Algorithmic Considerations and Validation," *Theoretical and Computational Fluid Dynamics*, Vol. 7, 1995, pp. 49–76.

[29] Pruett, C. D., "Spatial Direct Numerical Simulation of Transitioning High-Speed Flows," *Transitional and Turbulent Compressible Flows*, Vol. L. D. Kral, E. F. Spina, and C. Arakawa, editors, pp. 63-70, FED-Vol. 224, ASME, 1995.

[30] Zhong, X., "High-Order Finite-Difference Schemes for Numerical Simulation of Hypersonic Boundary-Layer Transition," *Journal of Computational Physics*, Vol. 144, August 1998, pp. 662–709.

[31] Zhong, X., "Leading-Edge Receptivity to Free Stream Disturbance Waves for Hypersonic Flow Over A Parabola," *Journal of Fluid Mechanics*, Vol. 441, 2001, pp. 315–367.

[32] Ma, Y. and Zhong, X., "Numerical simulation of receptivity and stability of nonequilibrium reacting hyperconic boundary layers," *AIAA 2001-0892*, 2001.

[33] Pai, S., "Magnetogasdynamics and plasma dynamics," Springer-Verlag/Prentice-Hall, 1962.

[34] Augustinus, J., Hoffmann, K. A., and Harada, S., "Numerical Solutions of Ideal MHD Equations for a Symmetric Blunt Body at Hypersonic Speeds," *AIAA Paper 98-0850*, 1999.

[35] Gaitonde, D. V., "Development of a Solver for 3-D Non-Ideal Magnetogasdynamics," *AIAA Paper 99-3610*, 1999.

[36] Mack, L. M., "Stability of Axisymmetric Boundary Layers on Sharp Cones at Hypersonic Mach Numbers," *AIAA Paper 87-1413*, 1987.

[37] Malik, M. R., "Numerical Methods for Hypersonic Boundary Layer Stability," *Journal of Comp. Phys.*, Vol. 86, 1990, pp. 376–413.

[38] Stetson, K. F. and Kimmel, R., "On the Breakdown of a Hypersonic Laminar Boundary Layer," *AIAA Paper 93-0896*, 1993.

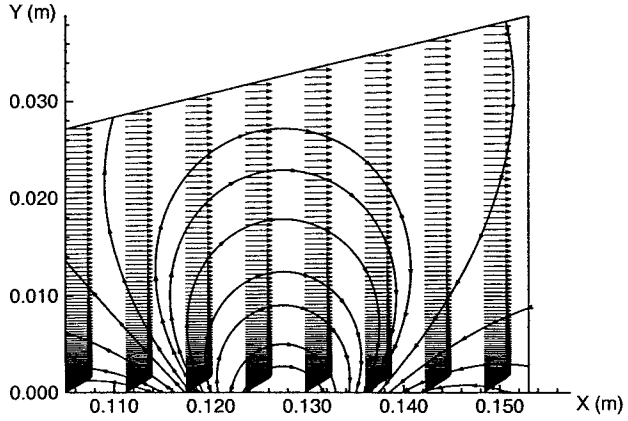

Figure 1: A schematic of a Mach 4.5 2-D weakly ionized flow over a flat plate in an imposed magnetic field.

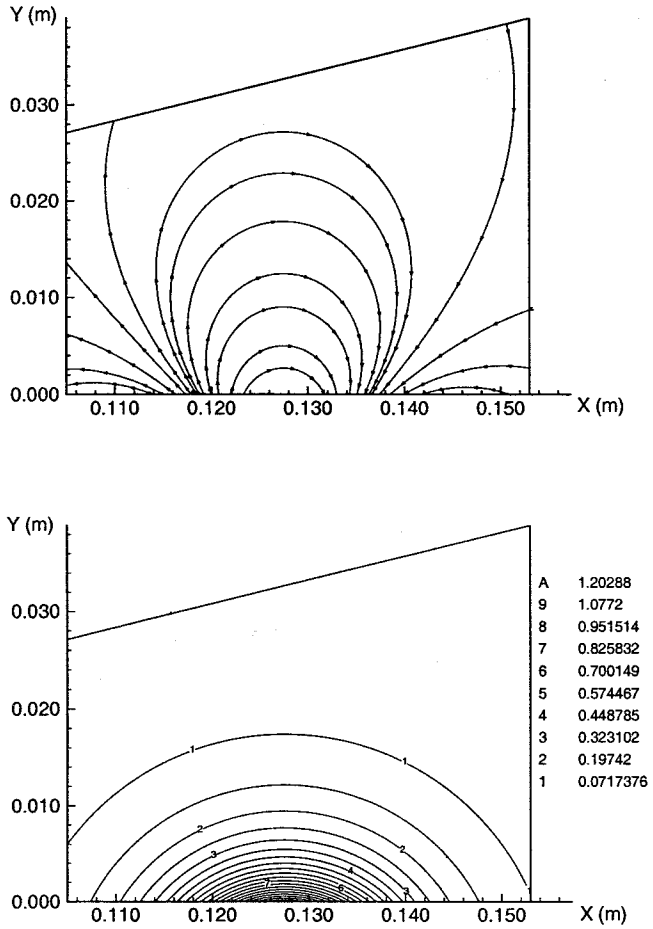

Figure 2: Magnetic field lines and the contours of B magnitude for Case I.a of two vertical magnetic dipoles in opposite directions with a relative weaker B field ($B_0 = 1.5 \times 10^{-4} Tm^2$, the dimensional x (and y) coordinates can be converted into nondimensional values by: $Re_x = xRe_\infty = 7.2 \times 10^6 x$).

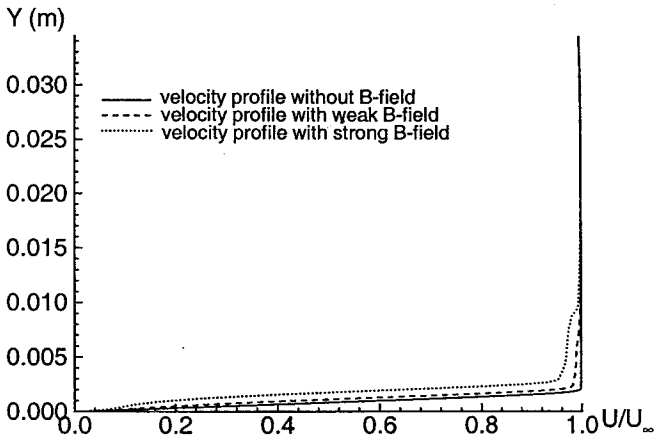

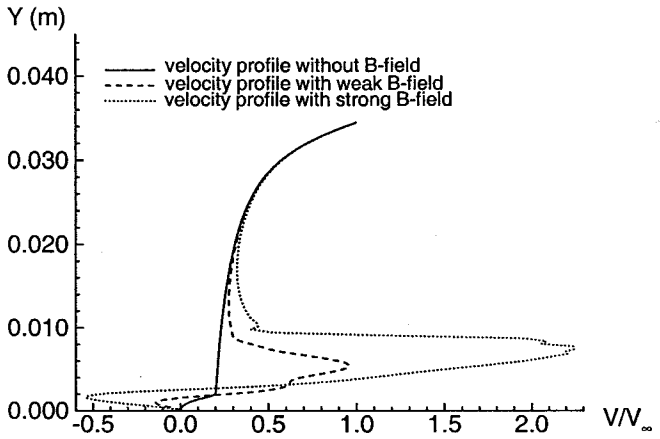

Figure 3: The profiles of streamwise and wall-normal velocity components affected by the weak and strong magnetic fields for Case I of the two vertical magnetic dipoles in opposite directions ($x = 0.1348m$).

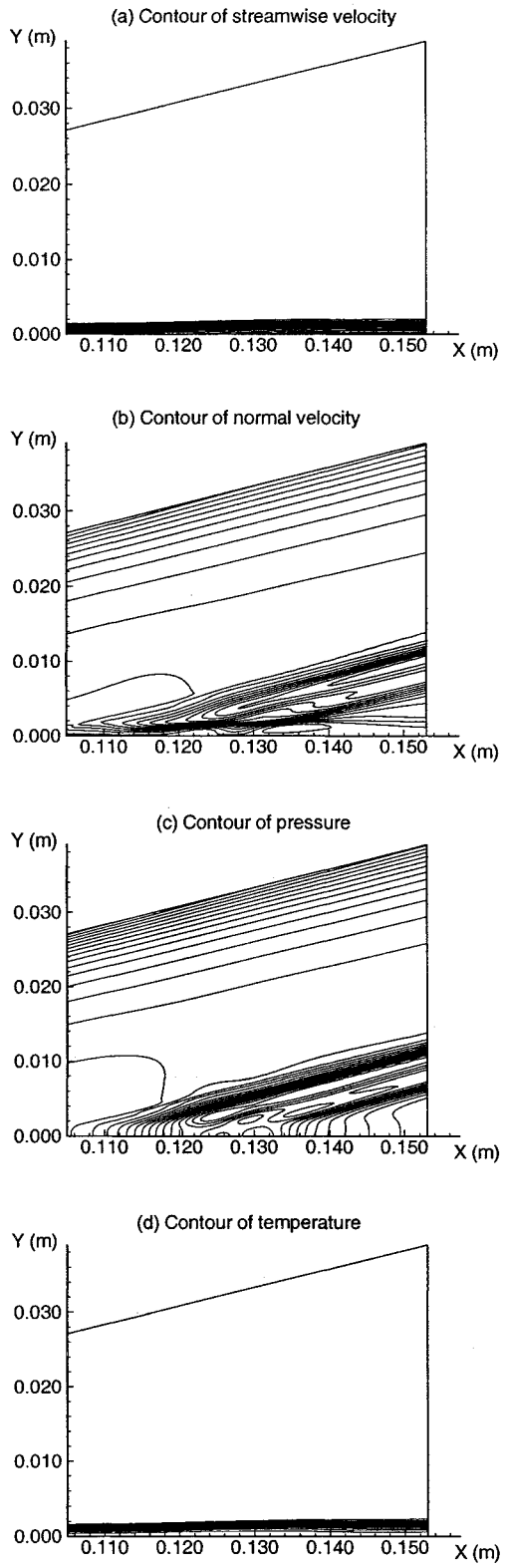

Figure 4: Contours of velocity components, pressure, and temperature for steady Mach 4.5 flow over a flat plate with a pair of magnetic dipoles in opposite directions for Case I.a of weak magnetic field.

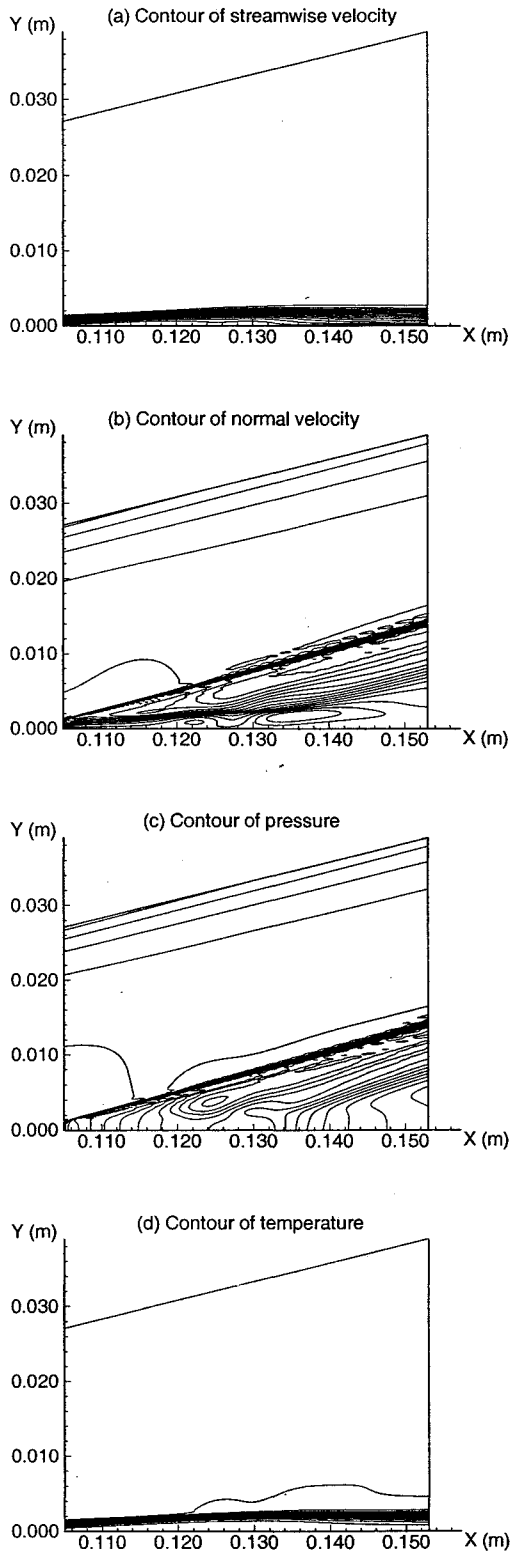

Figure 5: Contours of velocity components, pressure, and temperature for steady Mach 4.5 flow over a flat plate with a pair of magnetic dipoles in opposite directions for Case I.b of stronger magnetic field.

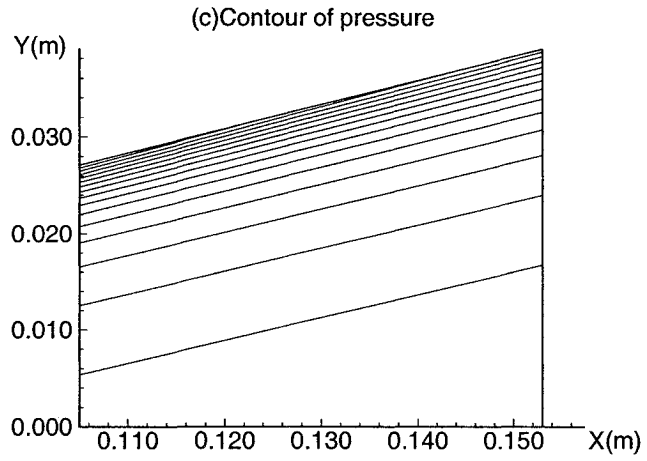

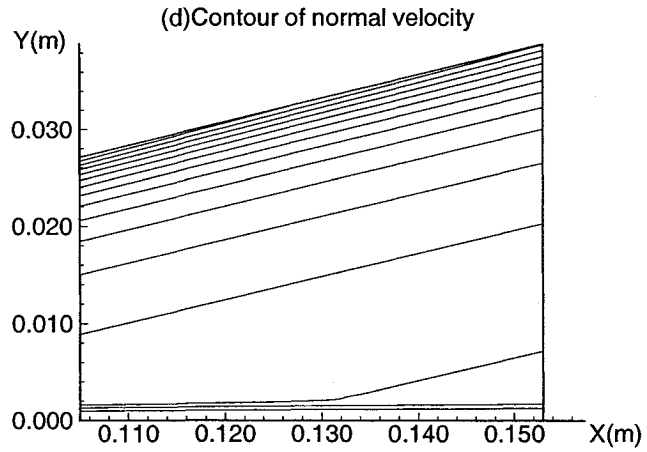

Figure 6: Pressure and normal velocity contours for a Mach 4.5 flow over a flat plate without MHD effect.

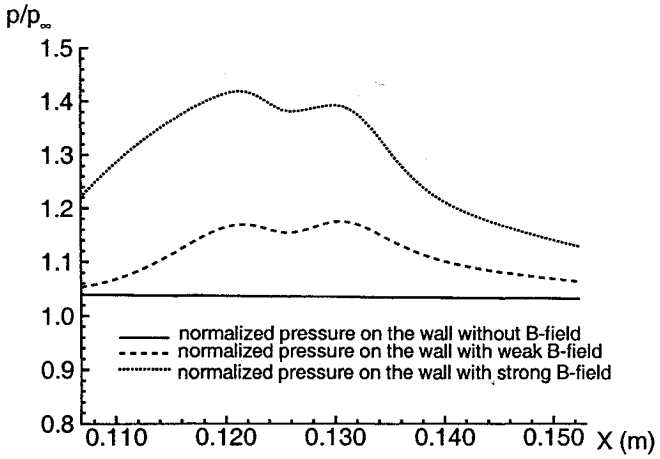

Figure 7: Comparison of the MHD effects on surface pressure distributions for Case I of a pair of vertical magnetic dipoles in opposite directions.

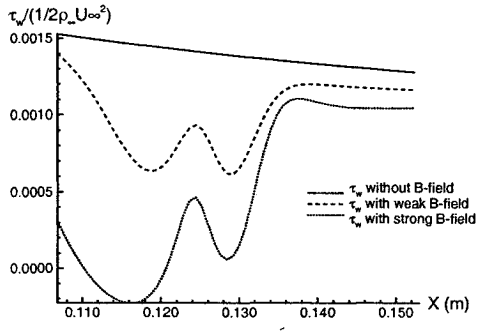

Figure 8: Comparison of the MHD effects on surface skin friction coefficient distributions for Case I of a pair of vertical magnetic dipoles in opposite directions.

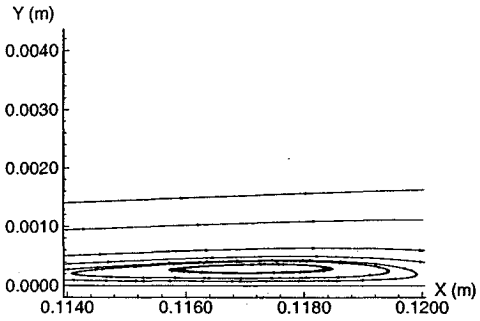

Figure 9: Streamlines showing a local separation bubble near the wall in Case I.b of two vertical magnetic dipoles in opposite directions with a strong magnetic field

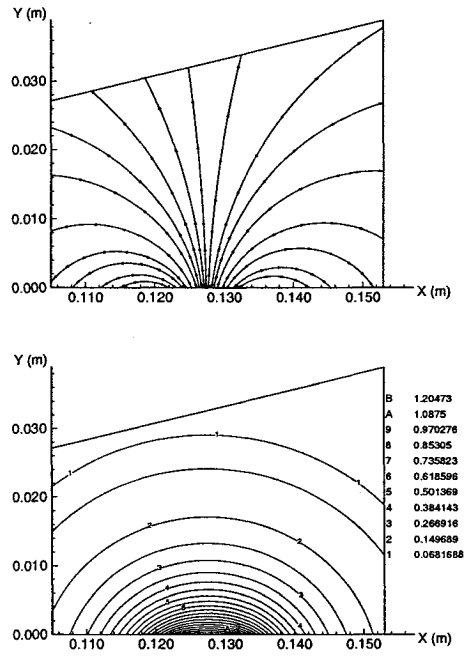

Figure 10: Magnetic field lines and the contours of B magnitude for Case II of two vertical magnetic dipoles in the same vertically upward direction with $B_0 = 0.45 \times 10^{-4} Tm^2$.

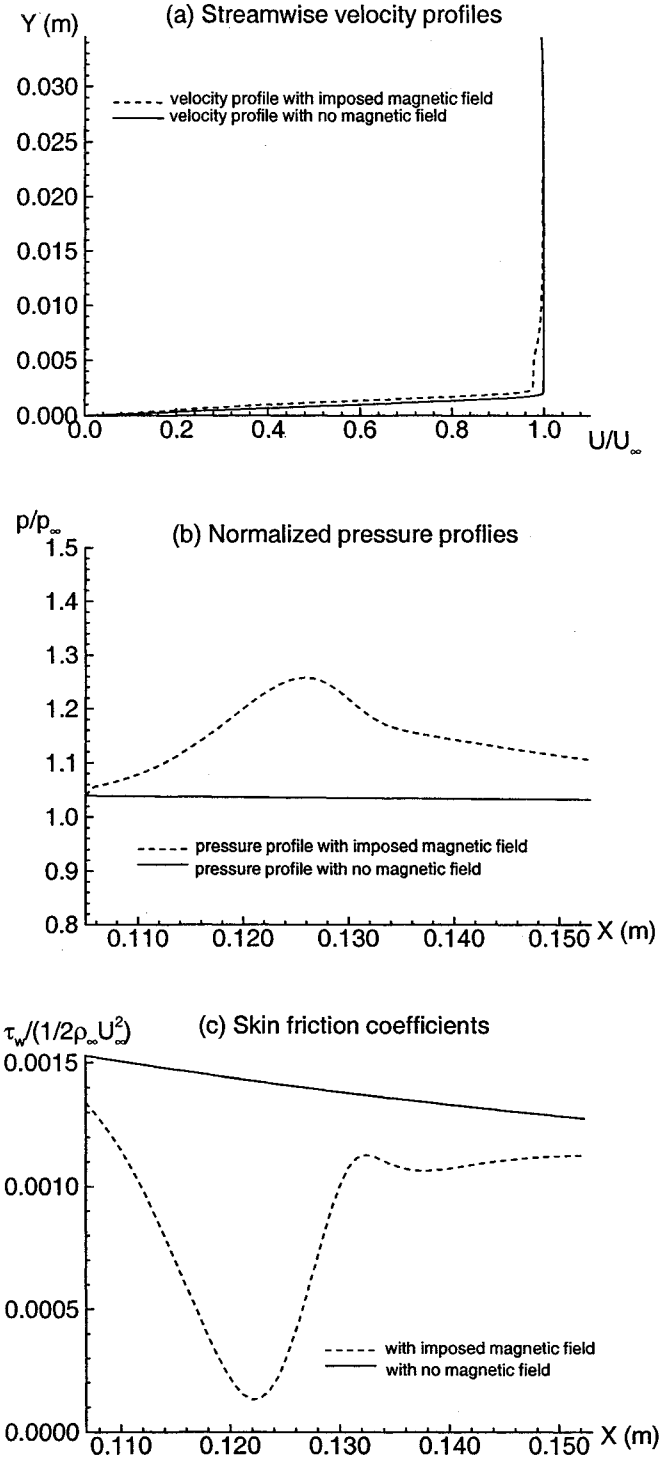

Figure 11: MHD effects on streamwise velocity, surface pressure, and skin friction coefficient distributions for Case II of a pair of vertical magnetic dipoles pointing in the same upward direction ($B_0 = 0.45 \times 10^{-4} Tm^2$).

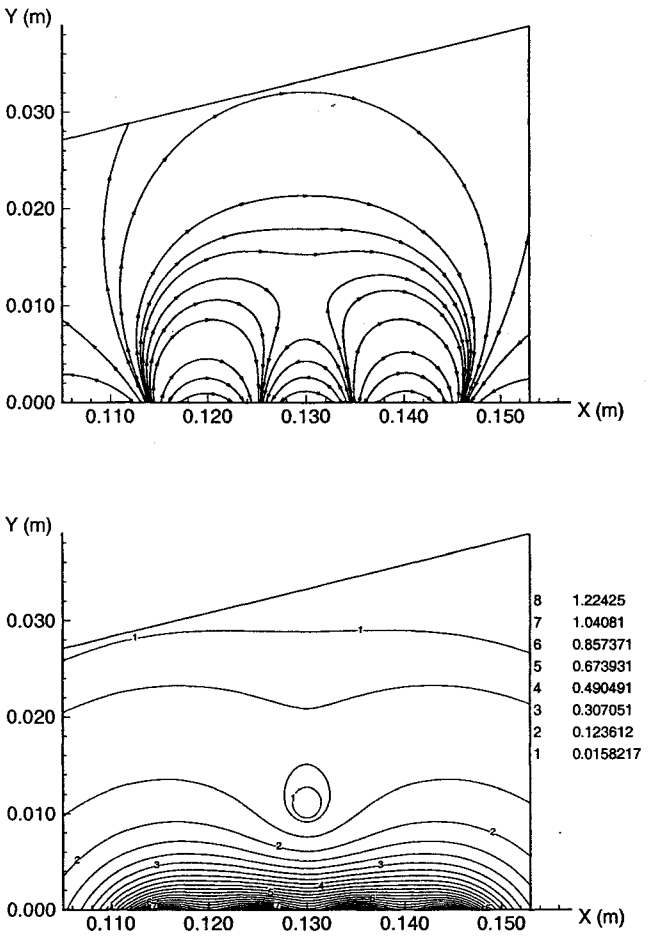

Figure 12: Magnetic field lines and the contours of B magnitude for Case III of four vertical magnetic dipoles pointing in alternating directions. All dipoles have $B_0 = 0.27 \times 10^{-4} Tm^2$.

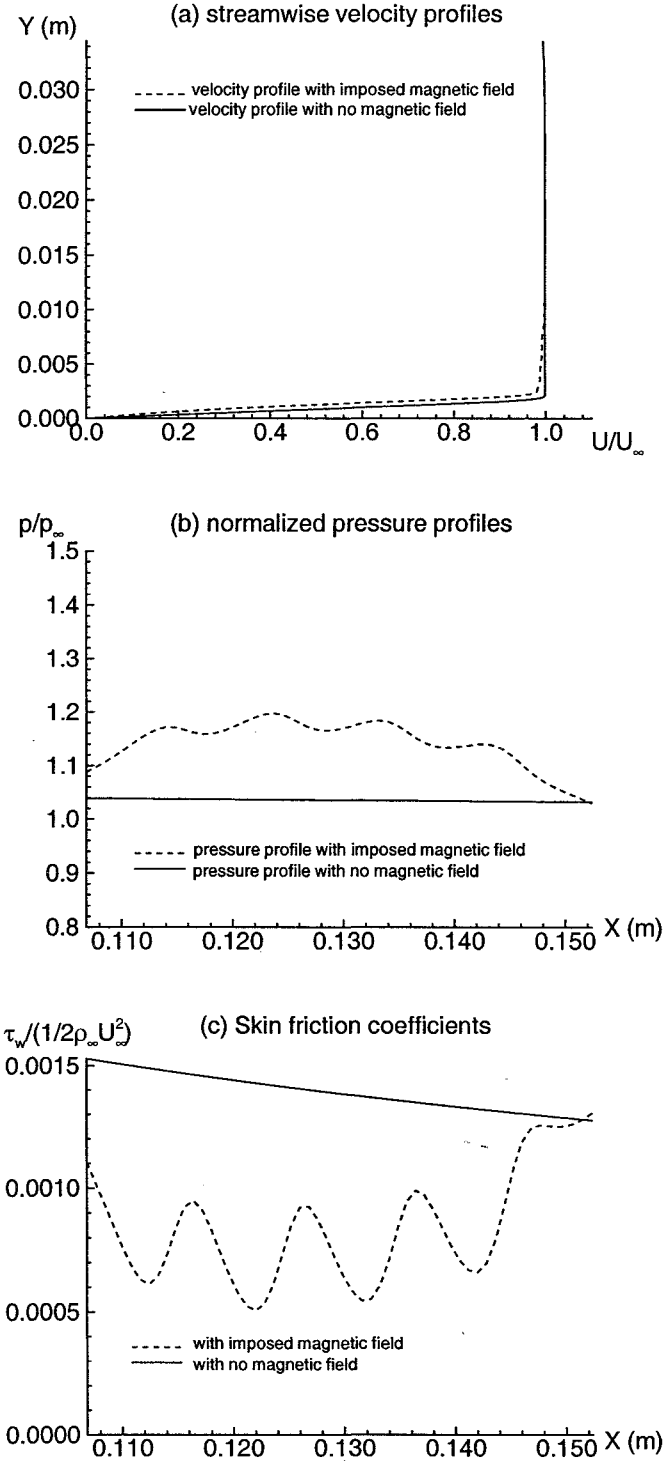

Figure 13: MHD effects on streamwise velocity, surface pressure, and skin friction coefficient distributions for Case III of four vertical magnetic dipoles pointing in alternating directions ($B_0 = 0.27 \times 10^{-4} Tm^2$).

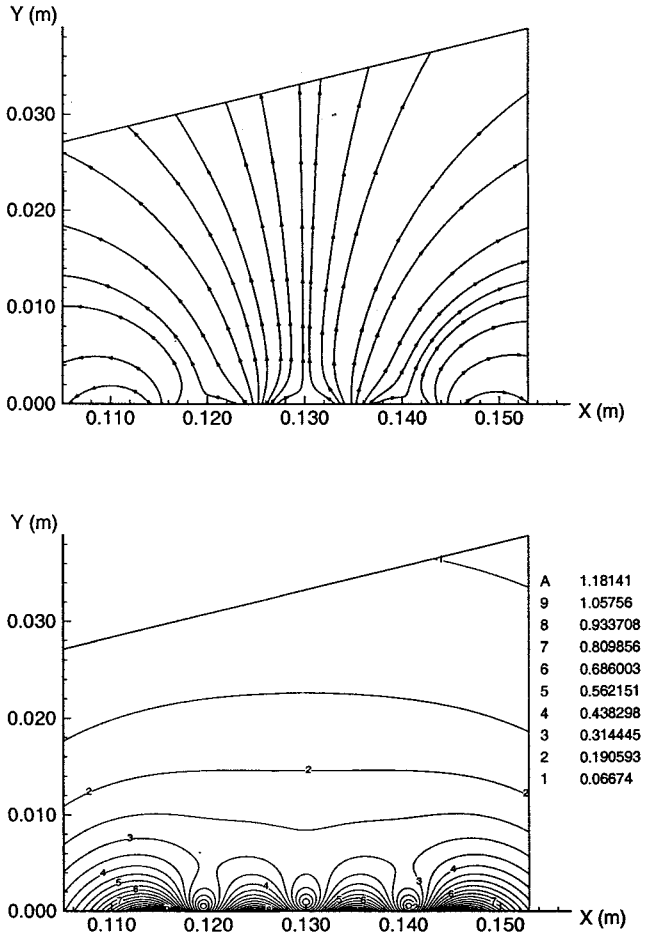

Figure 14: Magnetic field lines and the contours of B magnitude for Case IV of four vertical magnetic dipoles pointing in the same direction. All dipoles have $B_0 = 0.37 \times 10^{-4} Tm^2$.

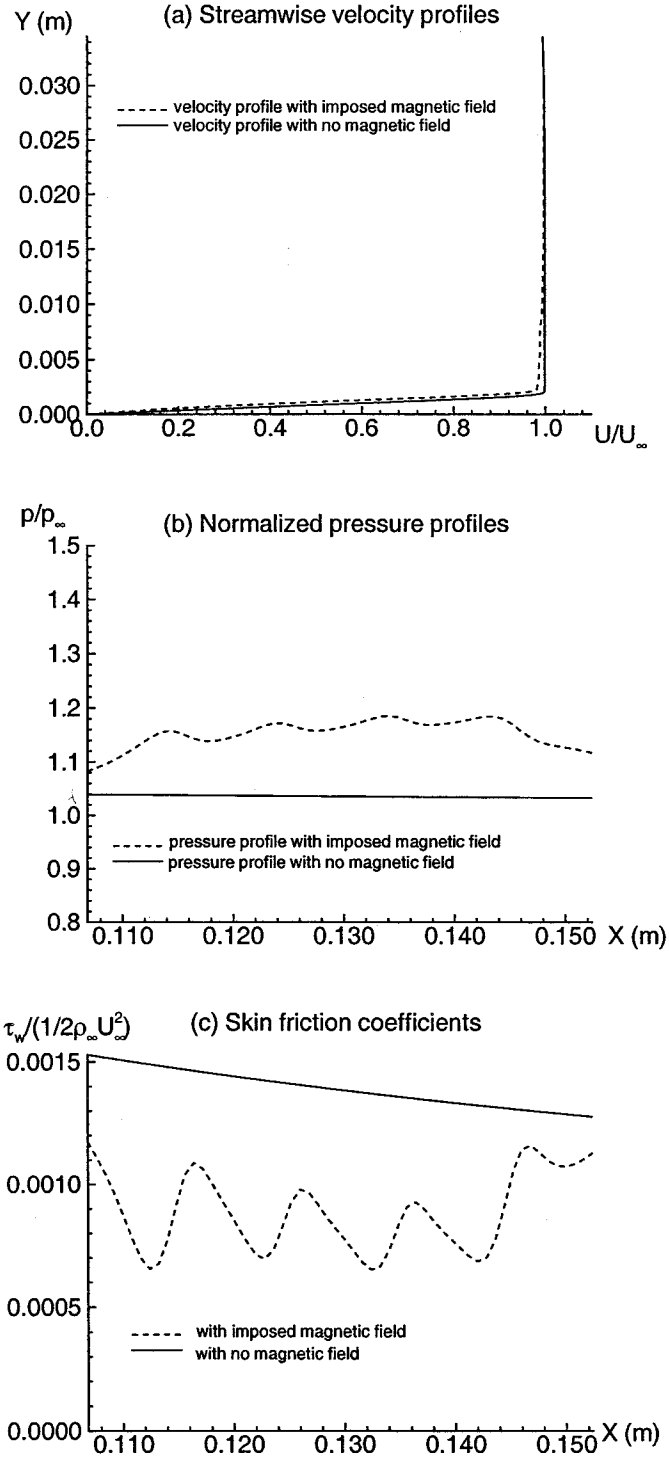

Figure 15: MHD effects on streamwise velocity, surface pressure, and skin friction coefficient distributions for Case IV of four vertical magnetic dipoles pointing in the same direction ($B_0 = 0.37 \times 10^{-4} Tm^2$).

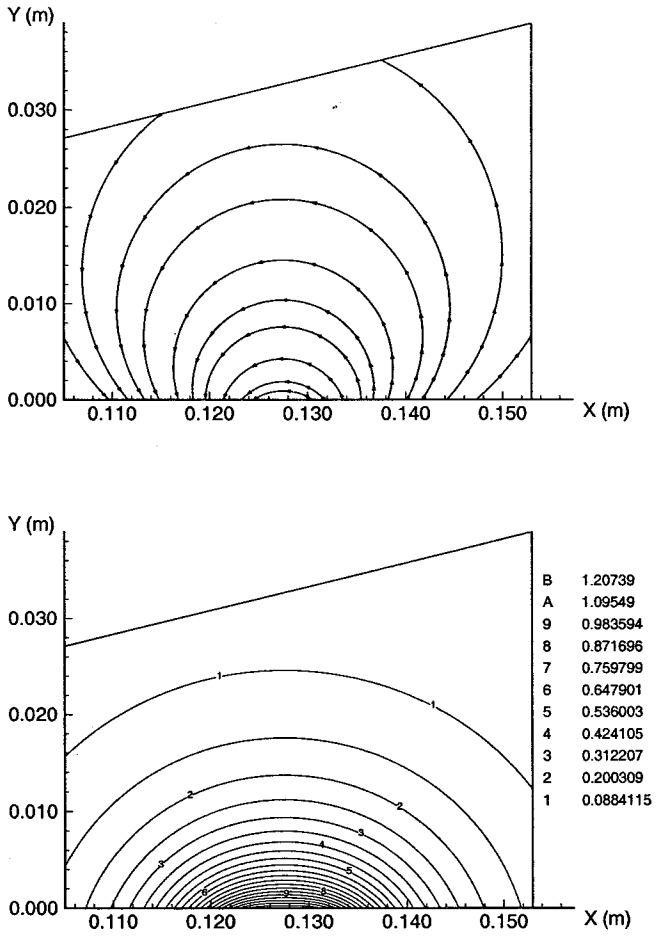

Figure 16: Magnetic field lines and the contours of B magnitude for Case V of two horizontal magnetic dipoles pointing in the same direction. All dipoles have $B_0 = 0.45 \times 10^{-4} Tm^2$.

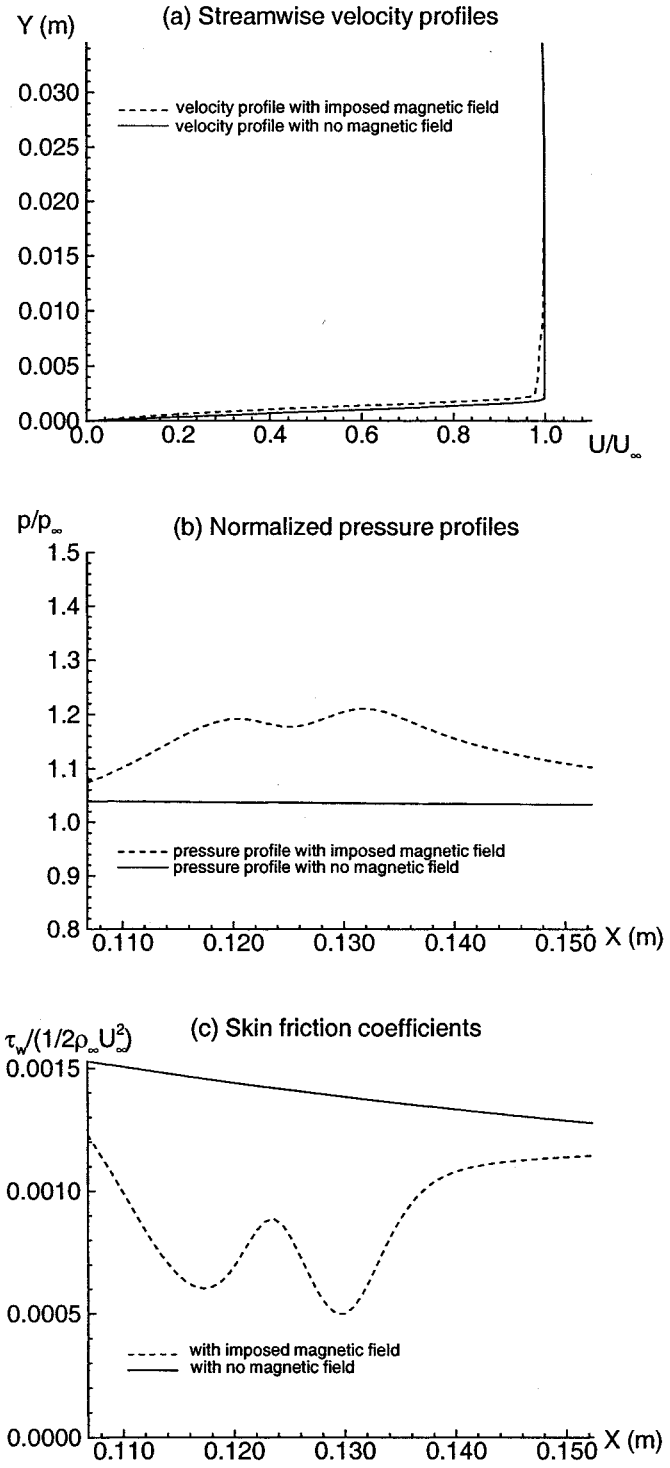

Figure 17: MHD effects on streamwise velocity, surface pressure, and skin friction coefficient distributions for Case V of two horizontal magnetic dipoles pointing in the same direction ($B_0 = 0.45 \times 10^{-4} Tm^2$).

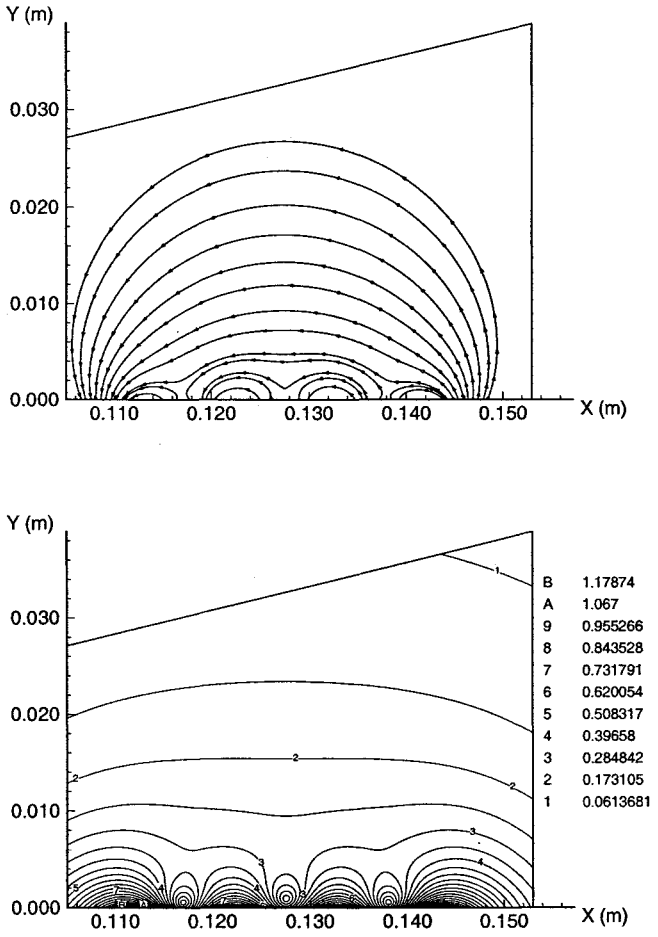

Figure 18: Magnetic field lines and the contours of B magnitude for Case VI of four horizontal magnetic dipoles pointing in the same direction. All dipoles have $B_0 = 0.35 \times 10^{-4} Tm^2$.

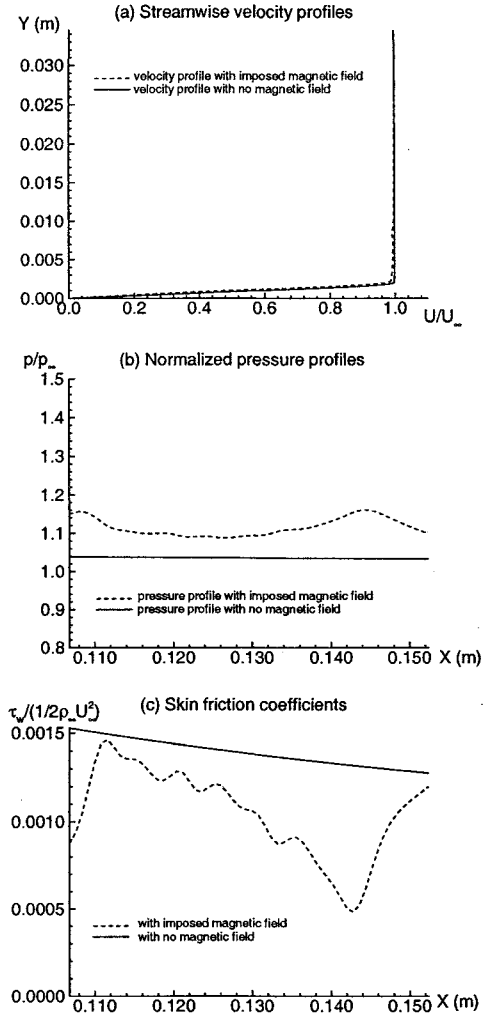

Figure 19: MHD effects on streamwise velocity, surface pressure, and skin friction coefficient distributions for Case VI of four horizontal magnetic dipoles pointing in the same direction ($B_0 = 0.35 \times 10^{-4} Tm^2$).

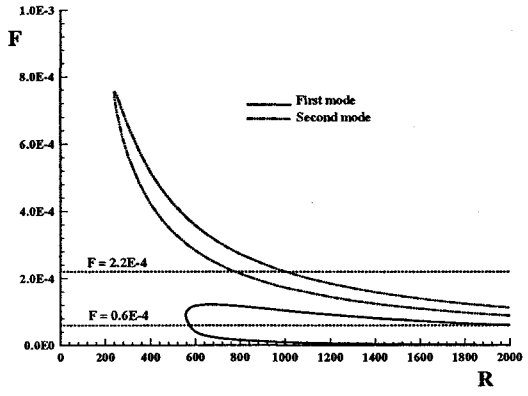

Figure 20: Neutral curves of stability (F vs R) for two-dimensional first- and subsonic-mode disturbances at $M_\infty = 4.5$ (Ma and Zhong, 2001).

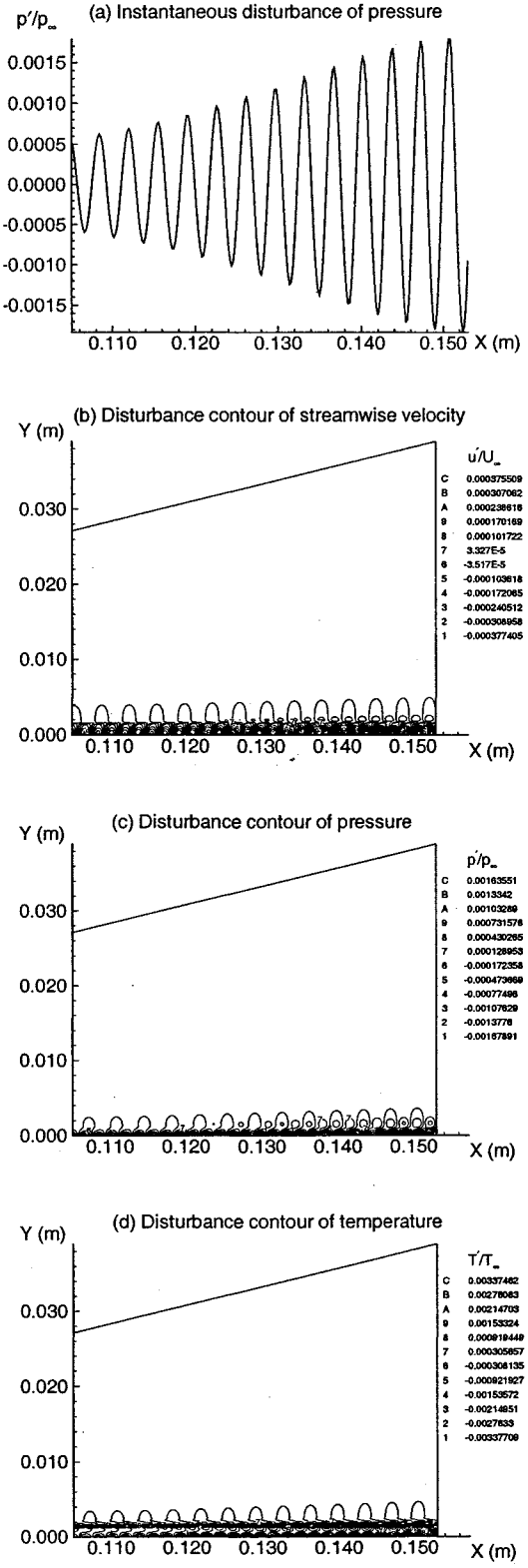

Figure 21: Second mode disturbances in a Mach 4.5 flow over a flat plate without MHD effect ($F = 2.2 \times 10^{-4}$) (Ma and Zhong, 2001).

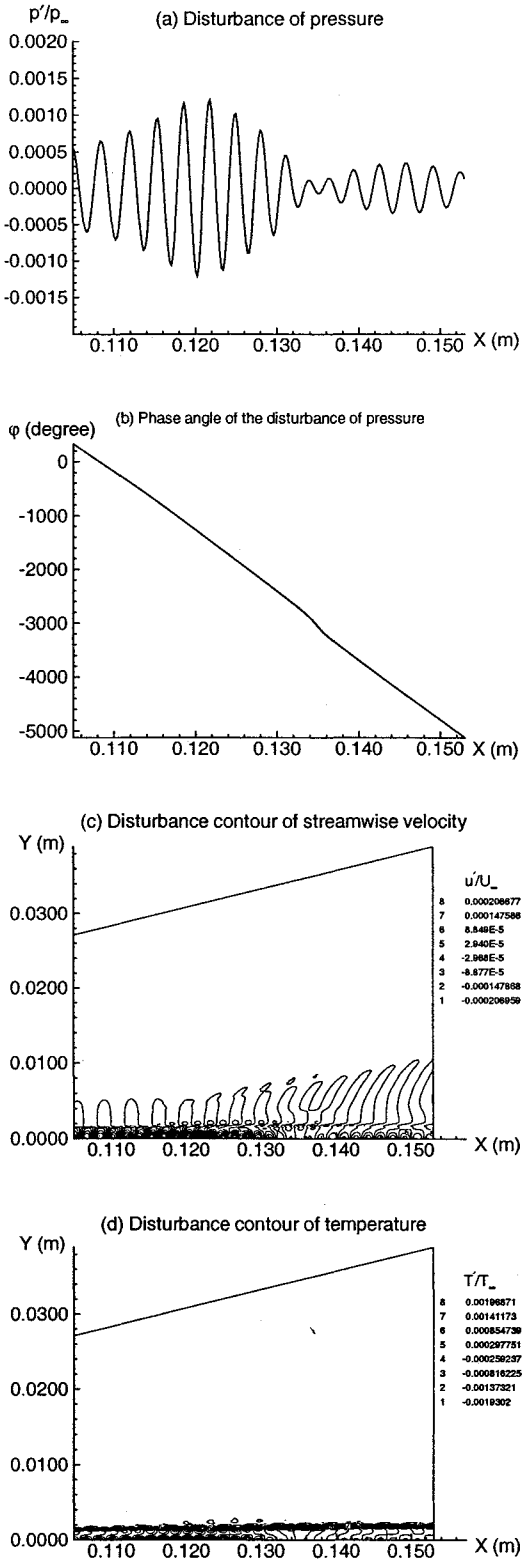

Figure 22: Second mode disturbances in a Mach 4.5 flow over a flat plate with a pair of magnetic dipoles in opposite vertical directions for Case I.a of weak magnetic field with $B_0 = 1.5 \times 10^{-4} Tm^2$.

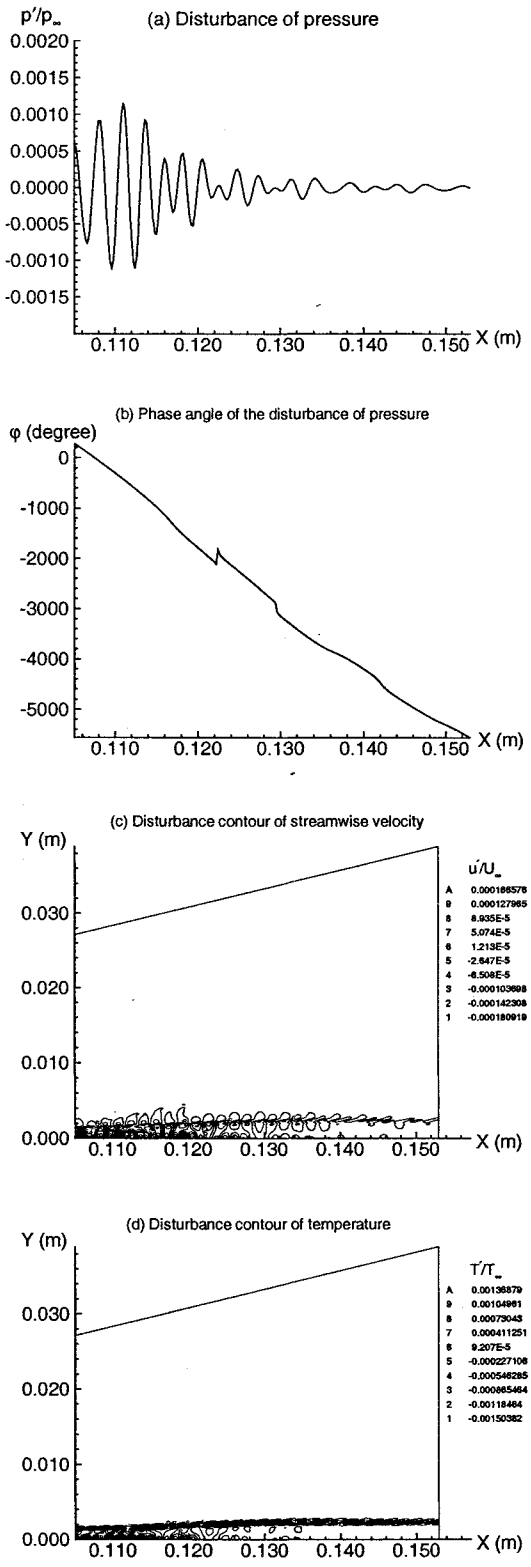

Figure 23: Second mode disturbances in a Mach 4.5 flow over a flat plate with a pair of magnetic dipoles in opposite vertical directions for Case I.b of strong magnetic field with $B_0 = 3 \times 10^{-4} Tm^2$.

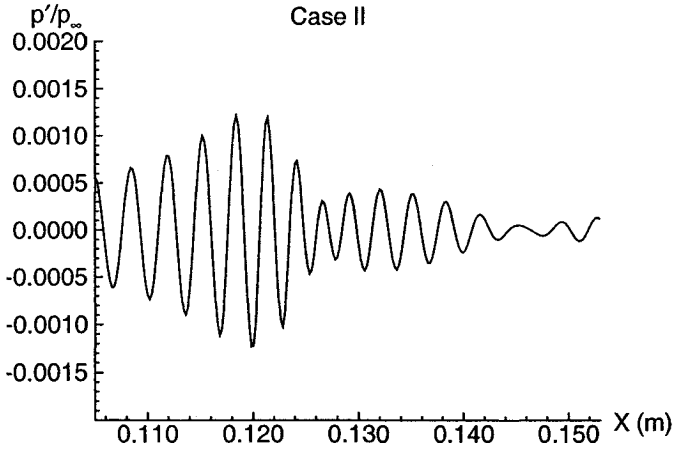

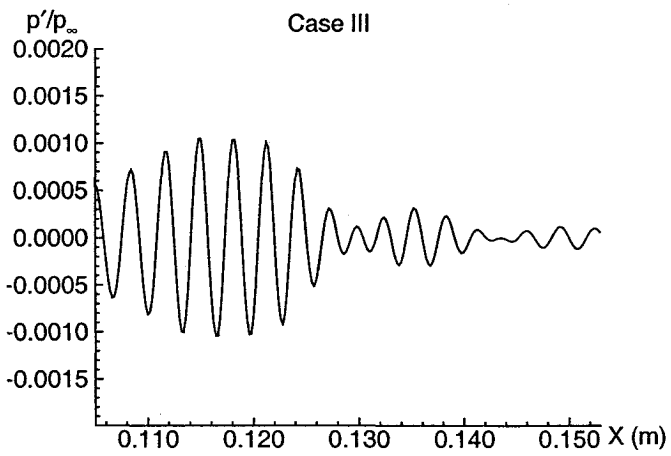

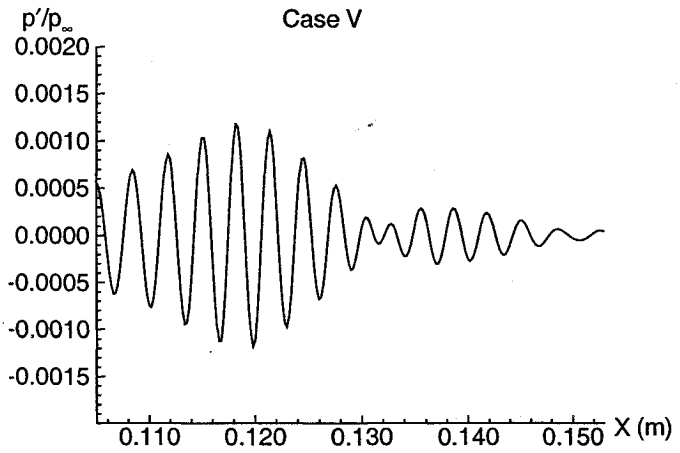

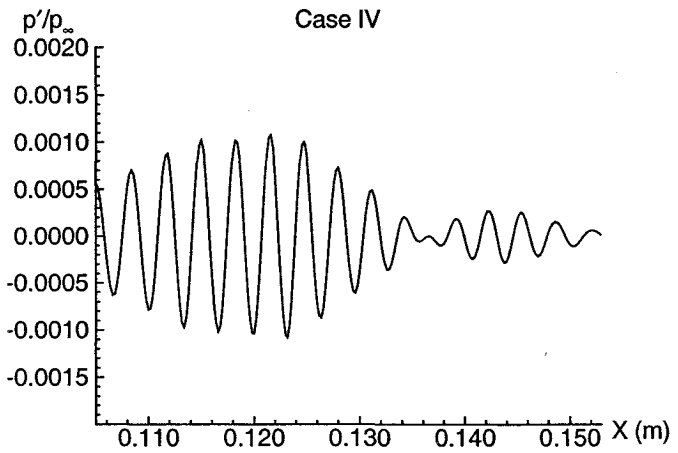

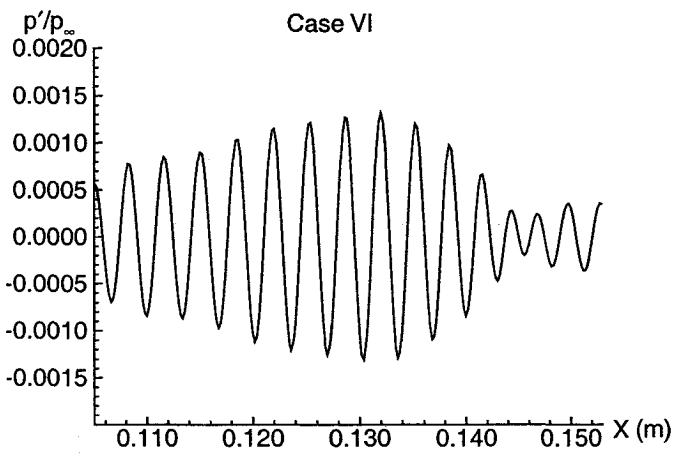

Figure 24: Second mode disturbances of pressure in a Mach 4.5 flow over a flat plate for three cases (Cases II, III, and IV) of different arrangements of vertical magnetic field.

Figure 25: Second mode disturbances of pressure in a Mach 4.5 flow over a flat plate for two cases (Cases V and VI) of different arrangements of horizontal magnetic field.

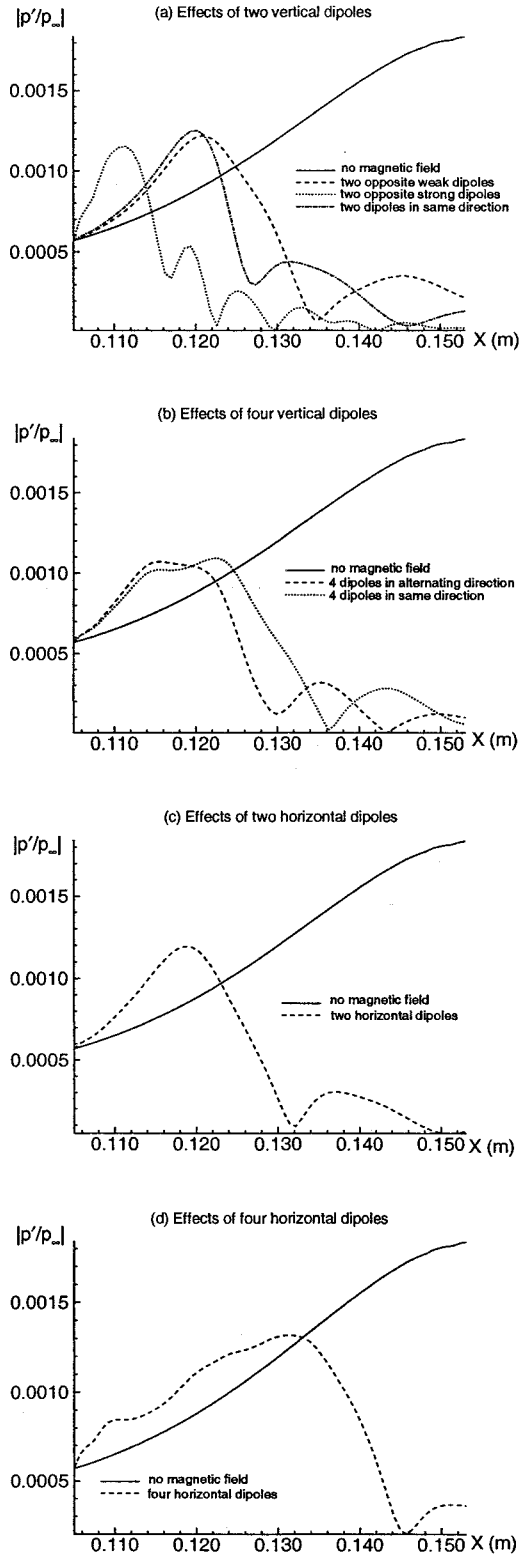

Figure 26: Effects of different magnetic dipole configurations on the magnitude of second mode disturbance of pressure.

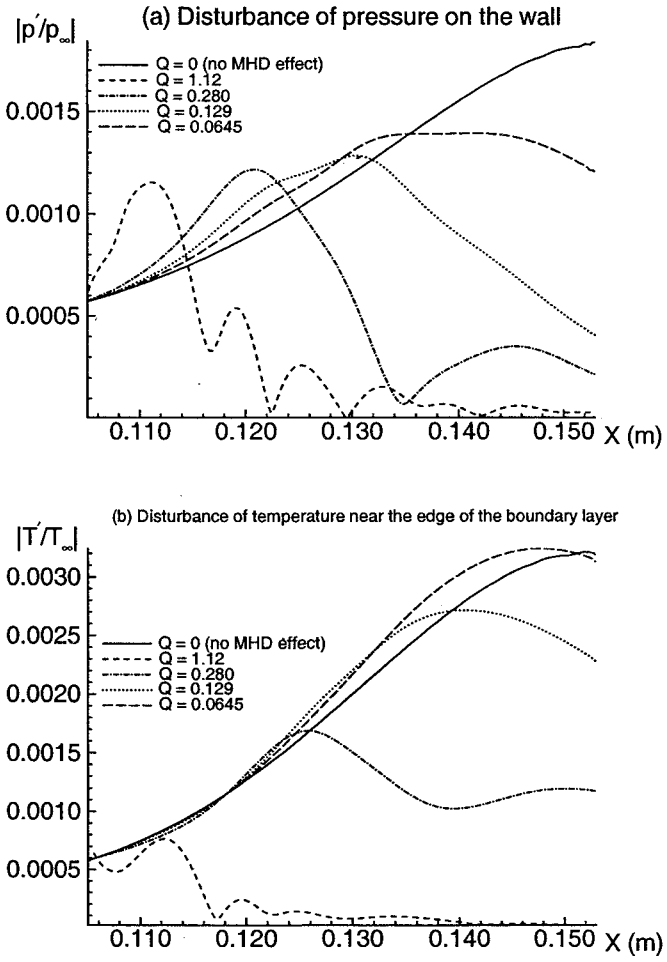

Figure 27: Effects of magnetic field strength on the second mode amplitude for the cases of the two vertical dipoles pointing in opposite directions with different strengths: (a) pressure perturbations on the wall, (b) temperature perturbations at a horizontal grid line of 40 grid points away from the wall.

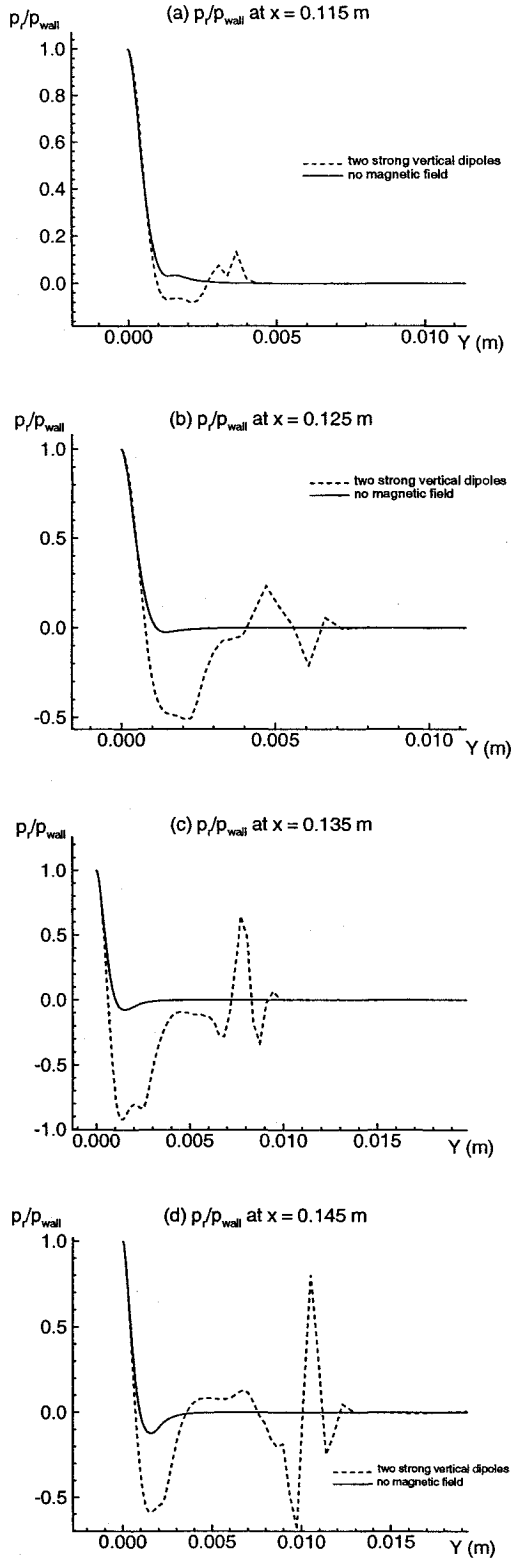

Figure 28: Evolutions of the real part of the eigenfunction of pressure disturbance under the influence of the two strong vertical magnetic dipoles (Case I.b).

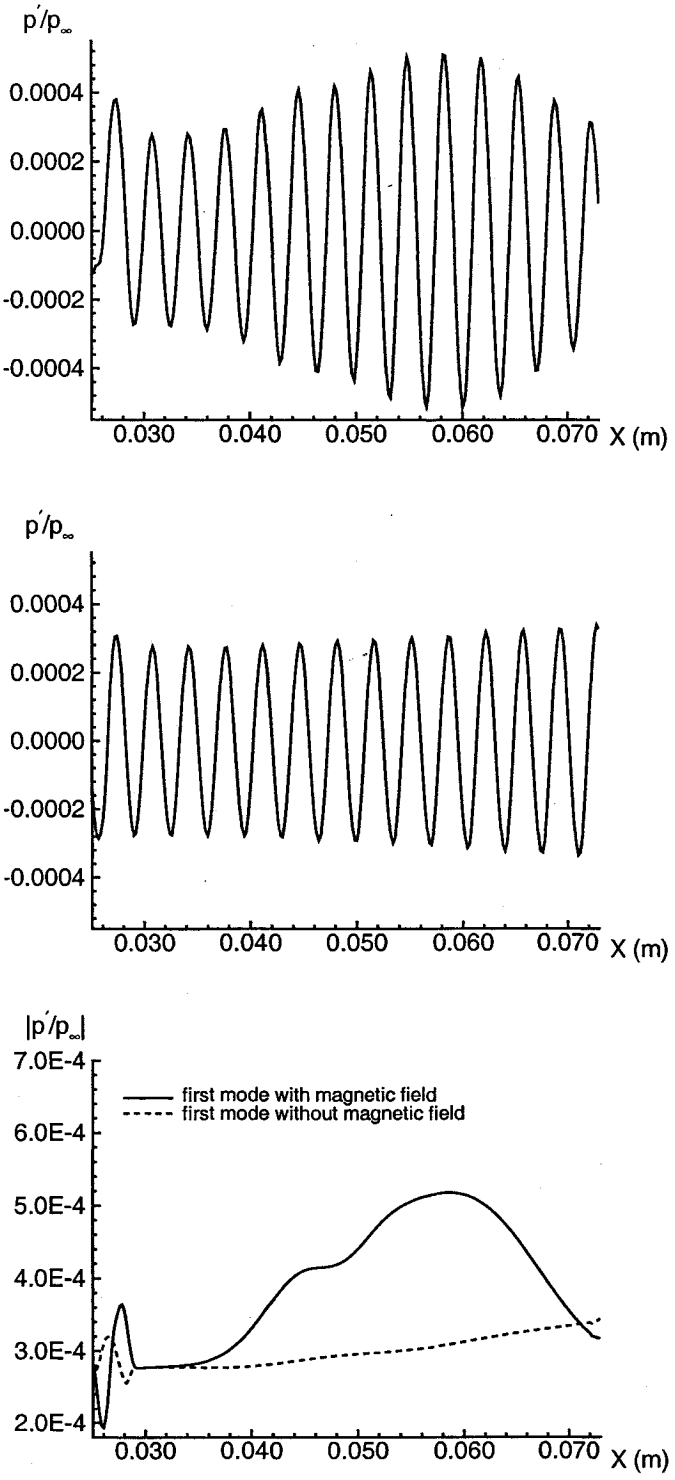

Figure 29: First mode disturbances in a Mach 4.5 flow over a flat plate with two vertical magnetic dipoles pointing in opposite directions. The nondimensional frequency is $F = 2.2 \times 10^{-4}$ (top figure: p vs. x plot with the magnetic field, middle figure: no magnetic field).